Biomaterials 136 (2017) 12–28

Contents lists available at ScienceDirect

Biomaterials

journal homepage: www.elsevier.com/locate/biomaterials

An interpenetrating network-strengthened and toughened hydrogel that supports cell-based nucleus pulposus regeneration

Yibo Gan [a], Pei Li [a], Liyuan Wang [a], Xiumei Mo [b], Lei Song [a], Yuan Xu [c], Chen Zhao [a], Bin Ouyang [a], Bing Tu [a], Lei Luo [a], Linyong Zhu [d], Shiwu Dong [e], Fuyou Li [f], Qiang Zhou [a, *]

[a] National & Regional United Engineering Laboratory of Tissue Engineering, Department of Orthopedics, Southwest Hospital, Third Military Medical University, Chongqing 400038, PR China
[b] College of Chemistry and Chemical Engineering and Biological Engineering, Donghua University, Shanghai 201620, PR China
[c] Department of Orthopedics, Xinqiao Hospital, Third Military Medical University, Chongqing, PR China
[d] Key Laboratory for Advanced Materials, Institute of Fine Chemicals, East China University of Science and Technology, Shanghai 200237, PR China
[e] Department of Biomedical Materials Science, School of Biomedical Engineering, Third Military Medical University, Chongqing 400038, PR China
[f] Department of Chemistry & State Key Laboratory of Molecular Engineering of Polymers, Fudan University, Shanghai 200433, PR China

ARTICLE INFO

Article history:
Received 2 December 2016
Received in revised form
6 May 2017
Accepted 8 May 2017
Available online 10 May 2017

Keywords:
Intervertebral disc
Nucleus pulposus
Hydrogel
Interpenetrating network
Minimally invasive surgery
Tissue engineering

ABSTRACT

Hydrogel is a suitable scaffold for the nucleus pulposus (NP) regeneration. However, its unmatched mechanical properties lead to implant failure in late-stage disc degeneration because of structural failure and implant extrusion after long-term compression. In this study, we evaluated an interpenetrating network (IPN)-strengthened and toughened hydrogel for NP regeneration, using dextran and gelatin as the primary network while poly (ethylene glycol) as the secondary network. The aim of this study was to realize the NP regeneration using the hydrogel. To achieve this, we optimized its properties by adjusting the mass ratios of the secondary/primary networks and determining the best preparation conditions for NP regeneration in a series of biomechanical, cytocompatibility, tissue engineering, and *in vivo* study. We found the optimal formulation of the IPN hydrogel, at a secondary/primary network ratio of 1:4, exhibited high toughness (the compressive strain reached 86%). The encapsulated NP cells showed increasing proliferation, cell clustering and matrix deposition. Furthermore, the hydrogel could support long-term cell retention and survival in the rat IVDs. It facilitated rehydration and regeneration of porcine degenerative NPs. In conclusion, this study demonstrates the tough IPN hydrogel could be a promising candidate for functional disc regeneration in future.

1. Introduction

Degenerative disc disease (DDD) is closely related to the process of aging and occurs in high incidence. It is one of the main causes of neck pain, low back pain and even disability, and it seriously affects the quality of life and working ability of patients [1]. With a rapidly aging population, DDD leads to a large burden on the public health and severe socioeconomic problems [2]. The common treatments of DDD include bed rest, physiotherapy, pain relief and surgery. However, these treatments do not overcome the pathological causes [3] and even result in some side effects. Therefore, there is an urgent need to find treatment strategies for DDD that focus on its etiology.

The intervertebral disc (IVD) has a confined structure, which is divided into three distinct zones: an inner hydrated gel-like nucleus pulposus (NP), a peripheral lamellar annulus fibrosus (AF) and superior and inferior cartilaginous endplates (CEPs) [4]. Fluid pressurization of the NP plays a major role in supporting axial spinal loads [5]. However, in degenerative discs, the NP fails to perform fluid pressurization because the NP is dehydrated; this dehydration causes significantly more axial compression on the NP and AF than usual, leads to an imbalance of the stress distribution on the IVD, and subsequently results in damage to the confined structure when the AF ruptures. Several attempts have been made to suture the AF defect to restore the confined structure and prevent disc reherniation [6,7]. However, most outcomes remain undesirable because it is difficult to achieve a strong long-term AF closure. DDD is believed to originate in the NP [8,9], in which gelatinous mucoid materials are replaced by fibrocartilages. Thus,

* Corresponding author.
E-mail address: zq_tlh@163.com (Q. Zhou).

http://dx.doi.org/10.1016/j.biomaterials.2017.05.017
0142-9612/

the regeneration of the degenerative NP is the key to the treatment of DDD. Owing to the limited regenerative capacity of nucleus pulposus cells (NPCs) [10,11], it 's hard to realize the self-renewal of the native NP. Tissue engineering and regenerative medicine (TERM) strategies have emerged as a promising solution to this issue [12,13]. Hydrogels are considered as potential candidates for the tissue-engineered nucleus pulposus (TE-NP) due to their similarities to the natural NP tissue, such as their hydrophilic and rheological properties [14,15]. Numerous types of hydrogels have been investigated for NP regeneration, such as alginate [16,17], chitosan [18,19], collagen [20,21], gellan gum [22,23] and composite hydrogels [24–26]. It has been illustrated that the ideal hydrogel for NP regeneration should satisfy the following requirements: it should 1) be injectable; 2) have a proper gelation rate to prevent leakage of the cells or gel after implantation, 3) have a high mechanical strength and suitable degradation rate, 4) it should provide swelling pressure at different loadings, 5) support cell proliferation and matrix deposition of encapsulated cells, and 6) be biocompatible to prevent adverse biological effects after implantation [27]. The NP bears highly compressive axial loads that are up to 70% of the exerted load on the spine and, in particular, it is subjected to higher compressive strains due to greater motion and disc space collapse during late-stage DDD [28]. Therefore, the mechanical properties are assumed to be the key parameters of hydrogels [29]. To achieve long-term regeneration, the implant should be tough enough to bear the axial compression in the early phase of regeneration, thus providing mechanical support and maintaining a three-dimensional (3D) template in the early stage of NP regeneration. Therefore, the toughness is an important mechanical criterion for assessing scaffolds for NP regeneration. However, most applied hydrogels are mechanically weak [30], which results in the collapse or even the bulging out of the structure during long-term compression and an inability to spatially and temporally support the NP tissue formation.

Several methods have been used to enhance the mechanical properties of hydrogels, e.g., fiber reinforcement; however, some ideal properties of the original materials were modified. Thus, it is difficult to improve the mechanical strength while retaining all the ideal properties of hydrogels, including their bioactivity and injectability, which limits the use of hydrogels for NP tissue engineering applications. Interpenetrating polymer network (IPN) hydrogels could be an attractive solution to this issue. IPN hydrogels are a type of unique “alloys” of crosslinked polymers. The synergetic effect of the different networks enables the IPN hydrogels to combine various advantages of the composite materials. Meanwhile, the toughness of the hydrogels can be tuned if the IPN hydrogel contains two types of independent networks, a rigid network and a flexible network, which makes IPN hydrogels especially suitable for load-bearing tissues. Previously, we prepared an IPN hydrogel composed of oxidized dextran (Odex), amino-modified gelatin and 4-arm poly-(ethylene glycol)-acrylate (4A-PEG-acr) [30]. This IPN hydrogel exhibited favorable cytocompatibility and feasible injectability. The most significant advantage was that the IPN hydrogel consisted of rigid 4A-PEG-acr networks and soft dextran/gelatin (Dex/Gel) networks, which made it possible to toughen the hydrogel by optimizing the ratio of the two networks. Before exploiting these gels for NP regeneration, it is necessary to improve the toughness and maintain the cytocompatibility.

The overall objective of this study was to realize the regeneration of the NP using the IPN hydrogel with an effective cell-based strategy. To achieve this, we optimized the mechanical properties and cytocompatibility of the IPN hydrogel by adjusting the mass ratio of two types of networks and determined the best preparation conditions that were most suitable for NP regeneration. First, the hydrogels were evaluated in terms of their mechanical properties (compression and shear) to achieve optimal performance. Second, the microstructures and hydration of the IPN hydrogel were examined. Third, the *in vitro* viability, proliferation, and extracellular matrix (ECM) deposition of the NPCs-hydrogel hybrid were evaluated. Finally, we explored the repair of the IVD *in vivo* by injecting the NPCs-hydrogel hybrid into NP defects of rats and porcine.

2. Materials and methods

2.1. Sample preparation

2.1.1. Cell isolation and culture

The animal use followed the guidelines of the local animal ethics committee [SYXK (YU) 2012-0012]. Primary NPCs were isolated from the IVDs of porcine (n = 5, male, aged ~3 months) from the Experimental Animal Center of Third Military Medical University, as previously reported [31]. In summary, the IVDs were obtained from the pigs until euthanasia via an overdose of pentobarbital (Aituo Chemical, Shenzhen, China) by intravenous injection, and then, the NP tissues were separated within 1 h after the surgery. The tissues were minced as finely as possible and treated with collagenase II (Sigma-Aldrich, USA) for 30 min under gentle shaking. After washing and centrifuging, the isolated cells were cultured in complete cell culture media [a DMEM/F12-based culture medium containing 10% FBS and 1% penicillin/streptomycin] in 5% CO_2 at 37 °C. Only for the *in vivo* study of rats in section 2.5.2, NPCs were isolated from lumbar discs and tail discs of Sprague-Dawley rats during CO_2 euthanasia (n = 10, male, aged ~9–12 weeks) in a similar manner. The primary passage 2 (P2) NPCs of porcine and rat presented adherently oval or spindle appearance, and were collected for the following experiments.

2.1.2. Preparation of Odex, amino-modified gelatin, and 4A-PEG-acr

Dextran (M_w 100,000) and gelatin were purchased from Sigma-Aldrich. Odex and amino-modified gelatin were synthesized using previously described procedures [30,32]. 4A-PEG-acr (M_w 10,000) was purchased from Jemkem Technology, Beijing, China. The resulting mixture was dialyzed (MWCO 7000 for Odex and amino-modified gelatin; MWCO 3500 for 4A-PEG-acr, JingKeHongDa Biotechnology Co., Shanghai, China) against distilled water to remove unreacted materials and other by-products. Finally, the mixture was lyophilized to obtain the final products.

2.1.3. Hydrogel formation

Dex/Gel/PEG hydrogels are prepared by a modified method from a previously reported process [30]. Briefly, dextran, gelatin, and PEG solutions, and I2959 solution (final concentration of 0.1 wt %, Sigma-Aldrich) in PBS were mixed to achieve a final polymer concentration of 10% in the gel. Then the pH of the mixture was adjusted to ~ 7.3–7.4 by triethylamine (Aladdin, Shanghai, China) and HCl. Then, the mixture was injected into a cylindrical mold (Ø = 10 mm, height = 5 mm) and incubated at 37 °C for 1 min, followed by exposure to 365 nm UV light (5 W cm^{-2}, UVATA, Shanghai, China) for 1 min (Fig. 1C). Our preliminary results indicated that when the mass ratio of the secondary/primary networks reached 1:1, the ductility was elevated relative to the hydrogel with a lower primary network proportion [30]. In this study, we continued to increase the primary network proportion to improve the toughness of the IPN hydrogel. However, the toughness of the IPN hydrogel could not be improved continuously when the mass ratio of secondary/primary networks was more than 1:8. Thus, the mass ratio of secondary/primary networks was set to 1:1, 1:2, 1:4 and 1:8. For the control groups, a single-network hydrogel of PEG and a Dex/Gel hydrogel were also prepared at a concentration of 10 wt%.

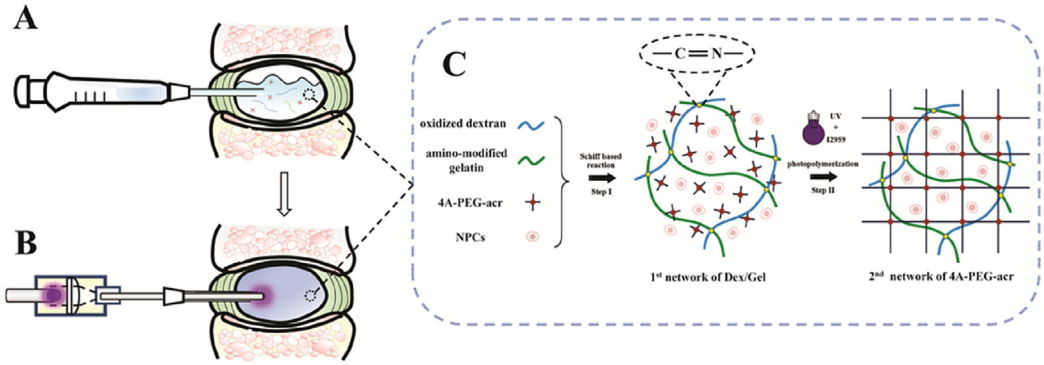

Fig. 1. Schematic diagram. (A) Injection of a cells-based interpenetrating network (IPN) hydrogel precursor into the NP cavity minimally. (B) Photopolymerization with a customized illuminating device for minimal invasion, composed of an UV flashlight, a light-focusing fiber lens and a fine optical fiber. (C) Gelation process of the IPN hydrogel including Schiff-based reaction between Odex and amino-modified gelatin, and photo-crosslink of 4A-PEG-acr.

2.1.4. NPCs encapsulated in hydrogels for in vitro experiments

For cell encapsulation, the P2 NPCs of porcine were premixed with precursor solutions at a density of 1×10^7 cells·mL^{-1}. The mixture was injected into the mold (Ø = 10 mm, height = 5 mm), where the cells were encapsulated in hydrogels after gelation. Next, the cell-seeded hydrogel was transferred to a custom-built bioreactor system [33]. Approximately 50 mL of the complete culture medium as described in section 2.1.1 was added into each culture chamber, which was followed by incubation in 5% CO_2 at 37 °C in the bioreactor with perfusion at a rate of 100 μL min^{-1} to promote ECM production and tissue remodeling [34].

2.2. Mechanical characterization

2.2.1. Compression testing

The mechanical compression properties were determined from the unconfined compression test. The gel dimensions were measured with calipers, and the hydrogels were compressed with a material testing instrument (ElectroForce® Load Frame Systems 3100 System, BOSE, USA) at room temperature. A flat, nonporous plunger was fitted with a 5N load cell. Each specimen was placed on the platforms, preloaded for 1 min and compressed at the strain rate of 1 mm min^{-1}. The Young's modulus, fracture stress, fracture strain and fracture energy were determined from a previous approach [35](n = 3).

2.2.2. Maintenance of hydrogel height under long-term cyclic compression

Hydrogels with a height of 0.5 cm were fabricated, as described, and they achieved equilibrium in the PBS bath at 37 °C after 3 days before undergoing cyclic loading. Next, the hydrogels were transferred to the bioreactor, which contained the loading cell for a long-term cyclic compression test. The loading protocol consisted of compression at 1 Hz between daily-applied strains of 5% and 20% for 8 h, which corresponds to 0.25 and 2 times the bodyweight for a disc of 1560 mm. During the loading phase, the heights of the relaxed hydrogels were observed by calipers before and after loading durations of 7 and 14 days, respectively. Each sample was measured from 3 directions (0°, 45°, and 90°; n = 3).

2.2.3. Viscoelastic properties

The viscoelastic behavior of the gels was measured by a rheometer (AH1000 Rheometer, TA Instruments, USA). Oscillation frequency sweep tests were performed, as previously described [36]. The storage modulus G″ represents the elastic property of the material, while the loss modulus G′ represents the viscous properties. The complex shear modulus |G*| is calculated from $(G'^2 + G''^2)^{1/2}$, which represents the resistance to shear-induced deformation. The phase shift angle is computed from $\delta = \tan^{-1}(G''/G')$ (n = 3).

2.3. Characterization of physical properties

2.3.1. Micromorphology

The hydrogels were first equilibrated in PBS for 24 h at room temperature and then frozen quickly by liquid nitrogen. The frozen specimens were cut into interior cross-sections with a thickness of 1 mm and lyophilized for 24 h. Then, they were coated with gold and imaged via a scanning electron microscope (SEM) at an accelerating voltage of 5–10 kV (S-3400N, Hitachi, Japan) (n = 3).

2.3.2. Mesh size evaluation

The average mesh size ξ was calculated from G' based on the rubber elasticity theory (RET) using the following equation [37]:

$$\xi = \left(\frac{G' N_A}{RT}\right)^{-\frac{1}{3}}$$

G′ is the storage modulus, N_A is the Avogadro constant, R is the molar gas constant, and T is the temperature (F).

2.3.3. Swelling under osmotic pressure

To study the swelling pressure of the hydrogels under load-induced pressures, similar to the IVDs, the hydration after equilibration was compared against solutions with different osmotic pressures, in a similar manner as the mechanical method [38]. Concisely, the hydrogels were lyophilized and then weighed. Next, they were placed in dialysis tubing (12,000 MWCO) and immersed in PEG (M_w 20, 000, Sigma-Aldrich) solutions with osmotic pressures between 0.3 and 6.9 atm (0.03–0.69 MPa), which is within the diurnal range experienced by human lumbar discs [39]. The samples were then removed from the dialysis tubing, weighed and dried. The NP tissues from the porcine lumbar IVD were tested as a positive control, and the overall hydration was determined, as previous described [40](n = 4).

2.3.4. Cell proliferation in the hydrogels

To investigate the cytocompatibility of the hydrogels, Cell Counting Kit-8 (CCK-8, Dojindo, Japan) were used to evaluate the proliferation of NPCs in the hydrogels on day 1, 4, and 7. The

medium was removed at each time point, and a fresh medium containing 10% CCK-8 was added for 3 h of incubation. The incubation solution was then transferred to a 96-well plate, and the absorbance was measured using a microplate reader at 450 nm (Model 550, Bio-Rad, USA) (n = 4).

2.4. NPCs encapsulated in hydrogels in vitro

2.4.1. Live & dead assay

The cell viability to the encapsulated NPCs in the different hydrogel types was evaluated with the LIVE/DEAD Viability Assay Kit (Invitrogen, USA), along with the manufacturer's instructions after 14 days of *in vitro* culture. Briefly, the cells-hydrogel hybrid was prepared and cultured, as indicated in Section 2.1.4. The culture medium was changed every day. Then, the hybrids were incubated with 1 mL of PBS containing 4 μM EthD-1 and 2 μM calcein AM. The hybrids were incubated for 40 min at 37 °C. After the samples were washed three times, the stained cells were visualized with a laser scanning confocal microscopy (LSCM. Zeiss 780, Germany). Image analysis was conducted by the Image J software (Wayne Rasband, National Institute of Health, USA). The cells in the different layers with fuzzy edges and a rounded shape were ignored during the counting procedure. Three randomly selected fields from three samples were used for quantification of the live (green) and dead (red) percentage for each group (n = 4).

2.4.2. Encapsulated cell morphology in the hydrogels

The 3D cell morphology in the hydrogels was observed after 14-days post-seeding using the LSCM. Briefly, the hydrogel samples were fixed in 1 mL of 4% formaldehyde for 30 min. Next, the encapsulated cells were permeabilized with 0.5% Triton X-100 (Sangon Biotech, China) for 30 min. Non-specific absorption was blocked using 3% bovine serum albumin (BSA, Sigma-Aldrich) for 1 h. After the samples were washed three times with PBS, the F-actin and nuclei were stained with rhodamine-conjugated phalloidin (160 nM, Invitrogen) overnight and 40, 60-diamidino-2-phenylindole (DAPI, 300 nM, Invitrogen) for 1 h. Confocal imaging was performed with the LSCM.

2.4.3. Histological analysis

Histological analysis was performed at 1, 14, and 28 days post-seeding. The samples were rinsed twice with PBS and fixed in 4% paraformaldehyde for 24 h. These samples were then embedded in paraffin and sectioned into 5-μm-thick sections. Serial sections were stained with hematoxylin and eosin (H&E), toluidine blue and Masson trichrome (n = 5). Cell-free hydrogels were stained as the negative control.

2.4.4. Biochemistry assays

For testing the proteoglycan deposits, the NPCs-seeded hydrogels were lyophilized at 7-, 14-, and 28-days post-seeding (n = 3). The samples preparation and DNA and glycosaminoglycan (GAG) content analyses were conducted, as previously described [41]. The HYP content was quantified according to methods adapted from Blumenkrantz and Asboe-Hansen [42]. The data were normalized to the DNA content of the sample.

2.4.5. Phenotype expression of NPCs encapsulated in hydrogels

To determine the sensing and response pattern of the NPCs in different hydrogels, the ECM-related gene expressions including aggrecan (ACAN), type IIα1 collagen(Col IIα1) and Sox-9 were assessed using real-time polymerase chain reaction (RT-PCR) at 7-, 14- and 28-days post-seeding (n = 3). GAPDH were used as the internal reference. RT-PCR was performed with a Power SYBR Green PCR Master Mix on a light cycle apparatus (Applied Biosystems 7500, Thermo Fisher Scientific, USA). All primer sequences were designed with Primer 5.0 (Table 1). Three replicate analyses were performed for each specimen, and three PCR runs were conducted for each gene. The level of the target gene expression was calculated as $2^{-\Delta\Delta}$Ct.

2.4.6. Immunohistochemical analysis

For histological analysis of the ECM deposition, cell-seeded hydrogels (n = 5) were harvested from 1-, 7-, and 14-days post-seeding and fixed with 4% formaldehyde for 24 h. After the samples were washed three times with PBS, the samples were fixed in paraffin medium and sectioned into 5-mm-thick sections. The samples were then stained with ACAN (1:400, NB120-11570, Novus Biologicals, USA) and type II collagen (Col II, 1:500, ab34712, Abcam, UK) following a standard immunohistochemistry staining procedure. The images were acquired by digital microscopy (CX41, Olympus, Japan).

2.4.7. Western blotting analysis

A semi-quantitative analysis was performed to test the ECM-related proteins secreted in the NPCs-seeded hydrogels via Western blotting, as previously described previously [43], using the following antibodies diluted in 3% BSA in TBST buffer: ACAN (1:1000, sc-16492, Santa Cruz Biotechnology, USA), Col II (1:5000), and Sox-9 (1:1000, sc-20095, Santa Cruz Biotechnology) antibodies and goat anti-mouse horseradish peroxidase-conjugated secondary antibody (1:2000, CW0102, Cwbiotech, China). Also, the protein level was quantified and normalized to the GAPDH bands by densitometry in the Image J software (n = 4).

2.5. In vivo studies

2.5.1. In vivo biocompatibility of implanted hydrogels

The hydrogels were implanted in dorsal subcutaneous pockets of Lewis rats (n = 9, 250–300 g, female) to gauge the fibrotic response to the hydrogels. The cell-free hydrogels were prepared as mentioned above. Hydrogels in each group were prepared in triplicate. After the rats were anesthetized with 50–80 mg kg^{-1} pentobarbital, a subcutaneous pocket on the back was created, and the hydrogels (Ø = 10 mm, height = 5 mm) were transferred into the pocket. The incision was then sutured using 5-0 nylon suture. The animals were sacrificed to determine the fibrotic response to the hydrogels after 8 weeks. The samples and surrounding tissues were fixed, sectioned, embedded and H&E stained.

2.5.2. Implantation of NPCs-based IPN hydrogel to rats' tails

2.5.2.1. Preparation of the NPCs that express luciferase. To visualize the cell retention and viability of the NPCs encapsulated in the IPN hydrogel when the hybrid was implanted into the IVD *in vivo*, rat NPCs expressing luciferase (NPCs-luc) were generated, as Aubrey T. Francisco et al. described [44]. The allogeneic rat P2 NPCs for rat implantation were isolated and cultured as presented in section 2.1.1. The VSV-G lentivirus vector that constantly expresses the luciferase2 transgene under the control of the EF1α promoter (Luc2-LVE) was obtained from Genechem, China. Briefly, the transduction medium was achieved by mixing the Luc2-LVE (80 × concentration) with culture media (5 μL per mL medium) containing 4 μg/mL polybrene (Sigma-Aldrich). Then, the adhering NPCs were incubated with the transduction medium for 24 h. Subsequently, the transduction media was removed, and the culture media was added for amplification. After the NPCs were harvested, they were tested by the luciferase reporter gene assay (excitation 562 nm). Monoclonal cells were selected and cryopreserved for the subsequent experiments.

Table 1
Real-time polymerase chain reaction primers.

Gene	GenBank ID	Sequence		Size
Aggrecan	NM_001164652.1	Forward	5′AGTCCACTGAGATCCTCTACTC3′	91bp
		Reverse	5′CCAAGAAGAAGGCCAACAAGGC3′	
Type II collagen α1	XM_001925959.4	Forward	5′ CAGGATGGGCAGAGGTATAATG3′	123bp
		Reverse	5′ GAGGCAGTCTTTCAGGTCTTC3′	
Sox-9	NM_213843.1	Forward	5′ TGCTGAATGAGAGCGAGAAG3′	97bp
		Reverse	5′ CGCGGCTGGTACTTGTAAT3′	
GAPDH	NM_001206359.1	Forward	5′ ACCTCCACTACATGGTCTACA 3′	91bp
		Reverse	5′ ATGACAAGCTTCCCGTTCTC 3′	

Primers for aggrecan, type II collagen α1, Sox-9 and GAPDH were designed from *Oryctolagus cuniculus* gene sequences obtained from the NCBI GenBank and RefSeq databases using Primer 5.0 software.

2.5.2.2. Preparation of illuminating device for minimal invasion and gelation efficiency testing. To induce photopolymerization of the hydrogels *in vivo* and prevent serious injury of the AF during the illumination, an illuminating device for minimal invasion was prepared, as shown in Fig. 1A and B. Briefly, an optical fiber (500 μm core, NA of 0.22, UVATA) was inserted through a 19G needle. A light-focusing fiber lens (UPUL, UVATA) was fixed at the outer end of the fiber and connected to a UV LED light (365 nm, UPF1, UVATA). To determine the gelatin volume with different illuminating times, the tip of the probe was immersed into 0.5 mL of the precursor, and the samples were illuminated with UV light. At various illuminating times, the samples were transferred to PBS and washed for three times. As the concentration was fixed at 10%, the density of the polymer precursor (ρ) was 1.1 g/mL. The photopolymerized hydrogels were then weighed by an electronic balance (W), and the volume of the hydrogels was calculated using W/ρ (n = 4).

2.5.2.3. Cells-hydrogel hybrid implantation and illumination in the rat IVD. Rats (Sprague-Dawley, n = 15, 250–300 g, female) were anesthetized with isoflurane, their skin shavings were preserved, and they were sterilized with iodophil. A 4-cm incision was made on the rat tail to expose the C3-C6 vertebrates (n = 5 per group). The NP of the C3-C4 disc was aspirated by a 19G needle. After each nucleotomy, the needle was removed, and a syringe was attached. The NPCs-luc were mixed with the above-mentioned IPN hydrogel precursors or PBS at a density of 1×10^7/mL, and 10 μL of the mixture was rapidly injected into the cannula with the syringe. Then, the syringe was removed, and the illuminating device was inserted into the center of the C3-C4 disc through the needle. The illuminating time was 20 min. The C4-C5 disc of the same tail only received the IPN hydrogel injection or the PBS injection (the sham treatment). Finally, the incision was closed with 5-0 nylon sutures.

2.5.2.4. Bioluminescent imaging. In vivo imaging of the rats with implantations of NPCs-luc were performed by bioluminescent imaging using the IVIS Spectrum (PerkinElmer, USA) on day 1 and day 28 after the surgery. The signal intensities were quantified with the Living Imaging software (PerkinElmer). In summary, the rats were anesthetized and injected intraperitoneally with D-luciferin (150 mg/kg, Sigma-Aldrich). The rats were imaged after 10-min injections. A defined region of interest (ROI) was drawn on the C3-C4 disc. The total luminescence within each ROI was obtained from the overlay luminescent images.

2.5.3. In vivo validation of the regenerative effect of IPN hydrogel in the porcine disc degeneration model

2.5.3.1. Surgical procedure of implantation. A porcine disc degeneration model was established with the nucleotomy, as previously described [45]. In summary, Bama minipigs (n = 3, aged~12 months, skeletally mature, weight 20–30 kg) were treated using an anterolateral retroperitoneal approach to the spine. The animals underwent partial nucleotomy under general anesthesia with isoflurane. Five lumbar vertebrae (L1–L5) were exposed, and L2-L3, L3-L4, and L4-L5 underwent partial nucleotomy with the 16G needle (removal of 0.05–0.1 g of the gel-like nucleus). Then, 0.5 mL of the cells-PBS mixture, the IPN hydrogel precursor alone, and the cells-IPN hydrogel mixture were injected into the L2-L3, L3-L4, and L4-L5 discs, respectively, and illuminated for 20 min based on the test presented in section 2.5.2.1. Finally, the incision was closed with 0 nylon sutures. The L1-L2 disc, which did not undergo nucleotomy, was used as a positive control. The allogeneic P2 NPCs of porcine were isolated from Bama minipigs (n = 3, male, aged ~3 months) and used as encapsulated cells here. The primary NPCs isolation and culture were presented in section 2.1.1. Minipigs without IVD operation (n = 3) were used as the preoperative group.

2.5.3.2. Magnetic resonance imaging. To evaluate the rehydration of the IVDs, the animals underwent T2-weighted sagittal magnetic resonance imaging (MRI, Megnetom Trio A Tim 3T, SIEMENS, USA) in the prone position after anesthesia at each set point (1 week, 3 weeks, 6 weeks and 12 weeks postoperatively). The IVDs were rated using a modified Piffirmann classification from 1 to 5, according to the signal intensity (SI) [46].

2.5.3.3. Micro-CT scanning. To quantitatively evaluate the disc height, Micro-CT scanning was performed, as previously described [17]. In brief, the spinal motion segments from L1-L5 were taken from the pig before the surgery and at the end time point after the operation. The samples were scanned with micro-CT (Skyscan 1272, Bruker, USA). The resolution of the scans was 20 μm, the exposure time was 2100 ms, the source voltage was 100 kV, the thresholding value was set at 155.3-D reconstructions, which were generated by the NRecon Reconstruction software (Bruker), and the height of the target tissue was measured by the DataViewer software (Bruker). The disc height index (DHI) was calculated by the percentage of the disc height to the length of the upper vertebral body and expressed as DHI (%) (post-injection DHI/pre-injection DHI).

2.5.3.4. Histological and immunofluorescent evaluation. To evaluate the regenerative result of the NPCs-IPN hydrogel implant *in vivo*, the samples were fixed in 4% paraformaldehyde, and samples of the spinal motion segments from L1-L5 were randomly selected for histological sagittal sections. Then, the serial sections were stained with H&E and toluidine blue to observe the disc structure and matrix distribution. The sections were visualized by a virtual microscopy slide scanning system (VS-120, Olympus, Japan). The degeneration grade was blindly scored by two independent observers, similar to a previous study [47]. Then, immunofluorescent evaluation of series of the sections was conducted with mouse monoclonal anti-aggrecan antibody (1:100) and rabbit monoclonal anti-collagen II antibody (1:100). Briefly, the sections were treated

with pepsin (1:10, Boster, China) for 30 min, then Triton X-100 (0.3%, ZSGB-BIO, China) for 10 min and incubated for 30 min with normal goat serum (ZSGB-BIO). Next, the sections were incubated with the primary antibodies at 37 °C for 1 h and at 4 °C for 12 h. Subsequently, the sections were incubated with Cy3.5- conjugated mouse anti-rabbit IgG (1:300, ZSGB-BIO) secondary antibodies and 488-conjugated rabbit anti-rabbit IgG (1:200, ZSGB-BIO) secondary antibodies for 1 h at room temperature. Thereafter, the cell nucleus was stained with DAPI solution for 10 min at room temperature. The immunostaining results were examined and photographed with the LSCM. For quantitative examination, the immunostaining results of the animal specimens were analyzed by the Image J software.

2.6. Statistical analysis

The quantitative data in this study are presented as the mean ± standard deviation. The SPSS statistical package 19.0 software (IBM, USA) was used for statistical analysis. The one-way analysis of variance (ANOVA) was applied to assess the statistical significance of the results between multiple independent groups. The repeated-measures ANOVA was adopted to analyze repeatedly measured data from the same sample at different time points in sections 2.2.2, 2.5.2.2, 2.5.3.2 and 2.5.3.3. The LSD *t*-test was used in the analysis of the two group parameters; differences were considered significant when the two-sided $p < 0.05$.

3. Results

3.1. Optimization of the mechanical properties of IPN hydrogels for NP implantation

In order to determine the proper scaffold to meet the mechanical requirements of the NP, the compressive properties, compression resistance and viscoelastic properties were selected as the parameters to optimize the IPN hydrogel. Fig. 2A shows the compressive process of three types of hydrogels. Fig. 2B shows the compressive stress–strain curves of the IPN hydrogel with different mass ratios of the dual networks. The compressive properties of the IPN hydrogels and SN hydrogels are listed in Table 2. The IPN hydrogel exhibited much higher toughness in compression compared to the Dex/Gel and PEG hydrogels. When compressed at a strain of 85%, the IPN hydrogel with a ratio of 1:4 exhibited structural integrity and a much higher horizontal expansion, which indicates its favorable compression resistance and high ductility. In contrast, a large fissure appeared on the edge of the PEG hydrogel, while the Dex/Gel hydrogel exhibited severe structure failure at the strain of 85% (Fig. 2A). As shown in Table 2, all the IPN hydrogels exhibited much higher ductility than the PEG hydrogel and much greater stiffness than the Dex/Gel hydrogel. There is a direct relationship between the mass ratio of the secondary/primary network and the compressive properties of the IPN hydrogel. The IPN hydrogel with a lower Dex/Gel proportion was relatively stiffer and more brittle, while those with higher Dex/Gel proportions were relative softer and more flexible. Interestingly, the IPN hydrogel with a ratio of 1:4 exhibited the highest fracture strain (1.97-fold vs. the PEG and 1.37-fold vs. the Dex/Gel, $p < 0.05$) and the highest fracture energy (2.60-fold vs. the PEG and 27.84-fold vs. the Dex/Gel, $p < 0.01$), demonstrating the high toughness of the hydrogel. Its modulus (15.86 ± 1.70 kPa) remained greater than the modulus of normal human NP tissue [48] (Fig. 2B). The result of the long-term compression resistance test (Fig. 2C) was in agreement with the compressive study. The height of the IPN hydrogel could be maintained under the compression as the IVD motion amplitude of high-intensity workers after 14 days. However, the height of the PEG hydrogel declined rapidly. This decline is possibly attributed to the brittleness, which resulted in increasing fissures on the hydrogel under cyclical compression and subsequently caused the local stress overload, leading to structural damage. For the Dex/Gel hydrogel, its relatively high flexibility could ensure that the height was maintained on day 7 (0.96-fold vs. the IPN hydrogel, $p > 0.05$), but its rapid degradation caused structural failure after 14 days' compression.

As shown in Fig. 2D–F, the viscoelastic properties of the IPN hydrogels with different network ratios were determined as G'/G″, |G*| (kPa) and δ (°) vs. frequency (rad^{-1}). The value of G'/G″ was higher than 1 in all groups, while the δ values of all the hydrogels were much lower than that of the normal NP (23–30° [49]) at the frequency range of 1–100 rad s^{-1} (Fig. 2D and E), which indicates the higher elastic properties of all the hydrogels compared to that of the natural NP. Overall, the hydrogels with a lower PEG proportion presented lower G'/G″ and δ values, which indicates more internal dissipation of the hydrogels with a lower PEG proportion under the shear. The |G*| quantity provides a measure of the shear stiffness of the material under dynamic conditions. The Dex/Gel hydrogel and the IPN hydrogels with a ratio of 1:4 and 1:8 had shear moduli within the range of those for the healthy NP (7–20 kPa [49]) at the frequency range of 1–100 rad s^{-1}, which demonstrates that the anti-shear capacity of these hydrogels was similar to that of the NP tissue (Fig. 2F).

All the mechanical tests results showed that the IPN hydrogel possessed high toughness and biomimetic shear modulus, which are beneficial to the anti-compression and anti-shear capacities of these hydrogels. These properties enabled them to maintain their 3D structure under the harsh mechanical environment in the IVD. Due to the excellent performance of the IPN hydrogel with a ratio of 1:4, it was selected as the optimal IPN hydrogel (IPN Opt) for the subsequent experiments.

3.2. Hydrogel microstructure and hydration characterization

As the mesh size was defined as the distance between valid cross-linking points of the hydrogel, the mesh size is mainly influenced by the cross-linking density at an identical swelling state [50]. Thus, the mesh size is related to the mechanical strength of the hydrogel. The cross-sectional interior of the IPN hydrogels exhibited a porous honeycomb-like structure under the same magnification (Fig. 2G1-6). As expected, the IPN hydrogel with a higher composition of PEG networks exhibited a compact and regular structure, while the IPN hydrogel with a higher composition of Dex/Gel networks showed a more porous and loose structure. Because the lyophilization process for SEM may have an impact on the internal fabric of the hydrogel, we quantified the mesh size using the rubber elasticity theory. The results showed that the mesh size was significantly higher for all the IPN hydrogels than the PEG hydrogels ($p < 0.05$) (Fig. 2H). The larger mesh size is relatively beneficial to cell survival due to the enhancement of the nutrient supply of encapsulated cells.

The hydration is an important function of the NP or the NP implant. A higher hydration is beneficial to fluid pressurization, which is needed to withstand compression for gel-like tissues in the NP cavity. Interestingly, the hydration of IPN Opt was close to that of the NP in the osmotic pressure level that corresponds to high mechanical loading (4.4 and 6.9 atm, $p > 0.05$) although it was significantly lower than that of the natural NP in the osmotic pressure level that corresponds to low mechanical loading (0.3 and 1.1 atm, $p > 0.05$), as shown in Supplementary data 1. Therefore, the NP-like hydration of the IPN Opt would bring high swelling pressure to the implant even when they were subjected *in vivo* to high mechanical loading.

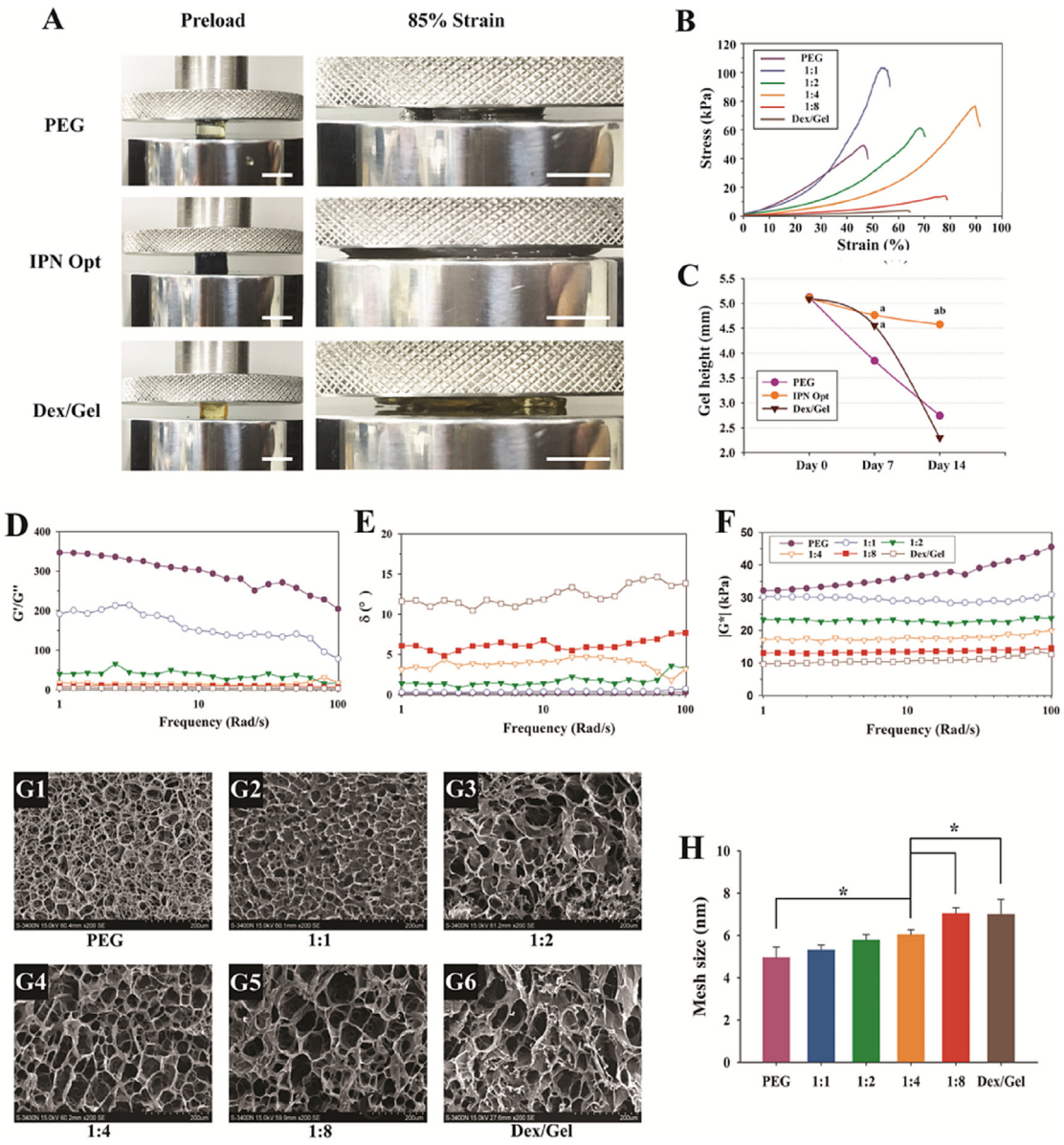

Fig. 2. Mechanical optimization of the IPN hydrogels. (A) The morphology of the PEG, optimal IPN, and Dex/Gel hydrogels at the compressive strain of 85%. Bar = 10 mm. (B) The compressive stress–strain curves of the IPN hydrogels with different mass ratios of secondary/primary networks. (C) The height variation of the hydrogels under the cyclical and high-amplitude compression on day 0, 7 and 14. (D–F) Plots of (D) storage modulus G'/loss modulus G'', (E) phase shift angle δ, and (F) complex shear modulus |G*| vs. frequency ($\omega = 1$–100 rad s^{-1}). (G) Scanning electron microscopy (SEM) micrographs of the internal structure of (G1) the PEG hydrogel, (G2-G5) 1:1, 1:2, 1:4 and 1:8 groups of the IPN hydrogels, and (G6) the Dex/Gel hydrogel. (Magnification: 400 ×, scale = 100 μm). (H) Histogram representing the mesh size of the hydrogels. The data are expressed as the mean ± standard deviation (SD). [a]$p < 0.05$ for comparison with PEG group at the same time point, [b]$p < 0.05$ for comparison with Dex/Gel group at the same time point. *$p < 0.05$. ($n = 3$).

Table 2
Mechanical properties of the tested hydrogels.

Gel type	Secondary/Primary Networks (Mass Ratio)	Modulus		Compressive failure properties		
		Young's Modulus (kPa)[a]	Shear Modulus (kPa)[a]	Fracture stress (kPa)[b]	Fracture strain (%)[c]	Fracture energy ($J \cdot m^{-2}$)[c]
PEG	–	59.42 ± 0.76	46.02 ± 9.23	53.31 ± 0.02	43.77 ± 2.59	9.12 ± 0.90
IPN	1:1	37.22 ± 11.59	25.62 ± 3.33	99.96 ± 9.45	50.83 ± 3.16	13.99 ± 2.51
	1:2	17.75 ± 4.31	21.14 ± 2.65	73.82 ± 11.73	70.09 ± 4.58	14.34 ± 0.84
	1:4 (Opt)	15.86 ± 1.70	19.28 ± 1.27	96.86 ± 19.76	86.42 ± 1.32	23.67 ± 4.38
	1:8	5.64 ± 0.62	12.56 ± 1.32	13.41 ± 1.49	72.45 ± 2.87	3.33 ± 0.36
Dex/Gel		2.22 ± 0.98	13.61 ± 3.41	3.93 ± 1.30	62.80 ± 0.54	0.85 ± 0.21

[a] IPN (1:4) was statistically significant from PEG hydrogel.
[b] IPN (1:4) was statistically significant from PEG and Dex/Gel hydrogel.
[c] IPN (1:4) was statistically significant from all other groups.

3.3. Cytocompatibility of the hydrogels

To determine whether the increase of the Dex/Gel network had a positive effect on the NPCs attachment, the CCK-8 assay was used. As shown in Fig. 3A, the test of cell proliferation in the hydrogels was performed on day 1, 4, and 7. During the tested period, the cell proliferation of the NPCs in the IPN hydrogels increased continuously. In contrast, the viability of the NPCs in the PEG hydrogel exhibited a decreasing trend as the incubation time increased and maintained a low level throughout. The elevated cell proliferation as the proportion of the Dex/Gel network increase is attributed to the presence of more cell adhesion sites in natural polymers. However, the Dex/Gel did not show the highest cell proliferation among all the groups, as expected. Although the proliferation of the NPCs in the Dex/Gel hydrogel was significantly elevated on day 4 compared to that on day 1 (1.10-fold, $p < 0.05$), the cell proliferation surprisingly decreased rapidly on day 7 compared to that on day 4 (0.55-fold, $p < 0.01$). This phenomenon is illustrated by the fast degradation rate of the Dex/Gel network, which could be determined from the following gross observation of the cell-seeded Dex/Gel hydrogel. In summary, the IPN hydrogel exhibited favorable cytocompatibility, and the IPN Opt could be used for the subsequent 3D culture experiments.

To detect the percentage of live cells, live/dead staining was used after encapsulation for 14 days (Fig. 3B–D). The majority of the NPCs (96.5 ± 2.0%) encapsulated in the optimal IPN hydrogels were green stained, which indicates the high viability of the NPCs after 14-days post-seeding (Fig. 3C). However, the percentage of live cells was statistically lower when the NPCs were encapsulated in the PEG hydrogels (26.8± 6.9%) compared to the IPN hydrogels after 14 days, indicating that PEG alone was not a proper carrier for cell delivery ($p < 0.01$, Supplementary data 2A). The inconsistent result with the cell proliferation assay was attributed to the high viability (92.4 ± 2.0%) of the encapsulated NPCs in the Dex/Gel hydrogel after 14 days (Fig. 3D), which indicates that the NPCs could survive in the non-degraded Dex/Gel hydrogel. However, the total amount of the living cells in the Dex/Gel hydrogels decreased significantly compared to that in the IPN hydrogel, as evidenced by the DNA content assay ($p < 0.01$, Supplementary data 2B); this indicates that a large number of cells flowed out due to the substantial degradation of the Dex/Gel hydrogel after 14 days, as revealed in Fig. 4A.

A series of confocal sections were then acquired from the top surface to a depth of 120 μm of the cells-IPN hydrogel hybrid to visualize the cell-matrix interactions (Fig. 3E.F). The actin of NPCs was stained red by rhodamine-labeled phalloidine while the cell nucleus was stained blue by DAPI. The blue-stained region outside the cells was unspecific staining background caused by the fluorescence absorption of the IPN hydrogel. After 14 days in culture, the encapsulated cells displayed a spherical morphology of the actin-stained cells and formed cell clusters (Fig. 3F), which is analogous to the NPCs in the natural NP tissue.

3.4. Histological analysis

The gross appearance of the cell-hydrogel hybrids was observed after 14 days' *in vitro* culture (Fig. 4A). The IPN and the PEG hybrids exhibited regularly cylindrical shapes. The PEG hybrid showed a higher swelling volume than the IPN hydrogel. In contrast, the Dex/Gel hydrogel was damaged and disintegrated during the culture period owing to its higher degradation rate.

To identify the histomorphological characteristics of the cell-seeded hydrogels, thin sections of each specimen were stained with H&E on days 4, 7 and 14. In the horizontal H&E stained sections of the cells-IPN hydrogel hybrids, a uniform and scattered distribution of the NPCs throughout the construct was observed on day 4 (Fig. 4C1). On day 7, cell clusters were formed (Fig. 4C2), and a change in the numbers and size of some cell clusters (yellow arrow) could be observed over the 14-day period (Fig. 4C1–4), which indicates NP-like cell organization has been established in the IPN hydrogel. In contrast, the encapsulated NPCs shrink, while some apoptotic bodies (red arrow) were observed in the PEG hydrogel during the culture period (Fig. 4B1–4). In the Dex/Gel hydrogel, the cell clusters (yellow arrow) were also formed during the culture period (Fig. 4D1-4). The histological result demonstrated that the IPN hydrogel is favorable for cell survival and the formation of the NP-like cellular organization.

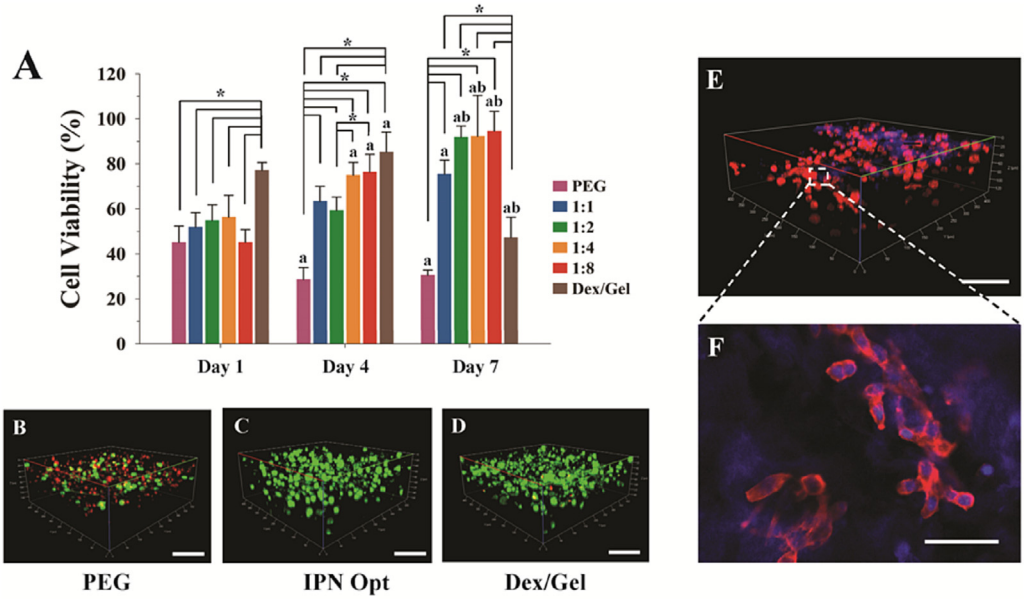

Fig. 3. Cytocompatibility measurement of the hydrogels. (A) The cell proliferation assay of encapsulated NPCs in the hydrogels on day 1, 4 and 7. (B–D) Live/dead staining of NPCs-seeded PEG hydrogels, optimal IPN hydrogels, and Dex/Gel hydrogels. (E–F) Morphologic observation of encapsulated NPCs in the IPN hydrogel. Magnification: 200 ×, bar = 100 μm. Data are expressed as means ± SD. *$p < 0.05$. [a]$p < 0.05$ for comparison with the same group on day 1, [b]$p < 0.05$ for comparison with the same group on day 4. ($n = 4$).

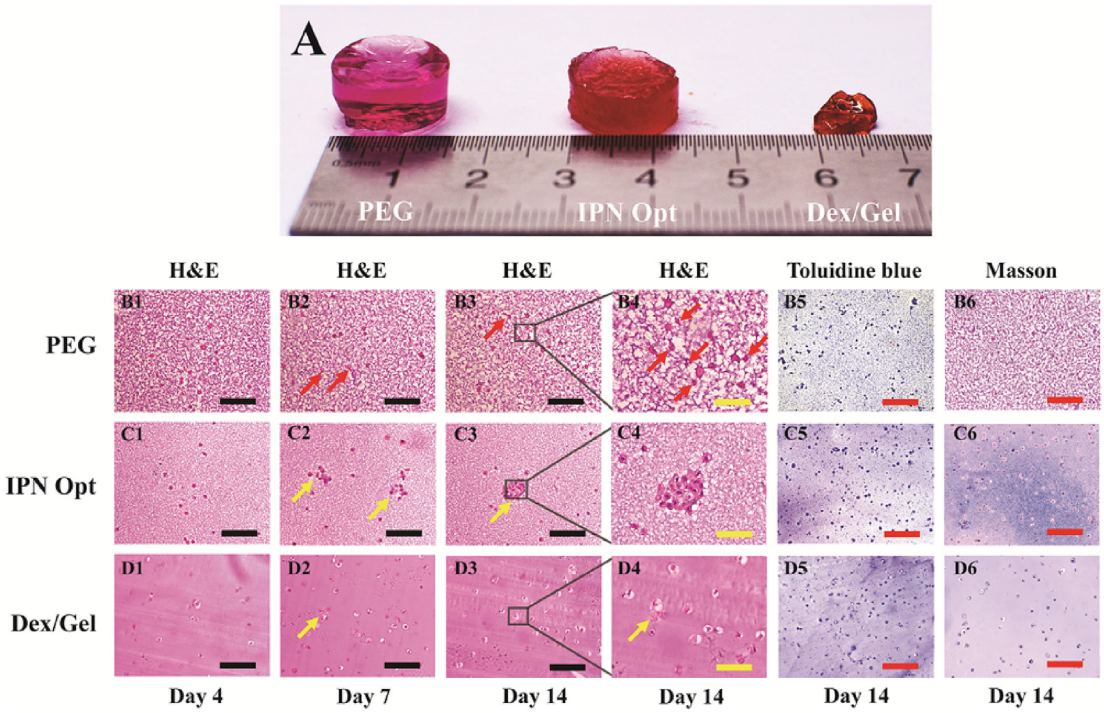

Fig. 4. Histological observation of the NPCs-encapsulated hydrogels. (A) Gross observation of the NPCs-encapsulated hydrogels after 14 days' *in vitro* culture. (B–D) Photomicrographs showed H&E, toluidine blue and Masson staining of the NPCs-encapsulated (B1-B5) PEG hydrogels, (C1-C6) the IPN hydrogels and (D1-D6) the Dex/Gel hydrogels on day 4, 7 and 14. The apoptotic bodies were indicated with a red arrow. The cell clusters were indicated with a yellow arrow. Black bar = 100 μm. Yellow bar = 50 μm. Red bar = 200 μm. (n = 5). (For interpretation of the references to colour in this figure legend, the reader is referred to the web version of this article.)

The gross organization of the dual networks in hydrogel scaffold could also be exhibited in the H&E section. The PEG hydrogel exhibited a structure of dense meshes. In contrast, the Dex/Gel hydrogel presented a homogeneous matrix organization. The IPN hydrogel, which combined the two types of networks, showed the meshes of PEG networks filled by the Dex/Gel matrix.

3.5. ECM deposition in the hydrogels

The accumulation of proteoglycans and the total collagen in the three types of hydrogels were examined using toluidine blue and Masson's trichrome staining. A higher deposition of proteoglycans was observed around the encapsulated cells in the IPN and Dex/Gel hydrogels (Fig. 4C5, D5) compared to the PEG hydrogel (Fig. 4B5). Similarly, a larger presence of the blue-stained dense collagen matrix was observed around the encapsulated cells in the IPN and Dex/Gel hydrogels (Fig. 4C6, D6), while a sparse presence of the collagen matrix was found in the PEG hydrogel (Fig. 4B6). It should be noted that the cell-free hydrogels (negative control) could be red-stained with Masson trichrome (Supplementary data 3). The quantitative amount of the total proteoglycans and the collagen was in accord with the histological result (Supplementary data 2C, D).

To detect the NP-specific ECM-related proteins expression and distribution in the hydrogels, immunohistochemistry staining of the NP-specific ECM of ACAN and Col II were performed in the cell-hydrogels hybrid on 4-, 7- and 14-days of post-seeding. As shown in Fig. 5B1 and E1, the ACAN, and Col II were limited intracellularly in the IPN hydrogels. As the culture time increased, these specific ECM-related proteins could be secreted to the pericellular region in the area of the cell clusters on day 7 (Fig. 5B2 and E2). On day 14, these proteins tended to deposit in broader regions in the IPN hydrogel (Fig 5B3, 4 and Fig 5E3, 4). In contrast, fewer cell clusters formed in the Dex/Gel hydrogel, and the expression of ACAN and Col II was less in the PEG and Dex/Gel hydrogels than in the IPN hydrogel at the same culture period. No positive signal was found in each of the negative control groups (Supplementary data 3).

To quantify the expression of the ECM-related protein in the hydrogel, the expression levels of specific NP-related proteins were tested by Western blotting (Fig. 5G–J). On days 4 and 7, a greater amount of the expressed ACAN, Col II, and Sox-9 was deposited in the IPN hydrogel and the Dex/Gel hydrogel compared to the PEG hydrogel ($p < 0.01$). Furthermore, the IPN hydrogel elicited a significant increase in the protein expression levels of ACAN, Col II, and Sox-9 on day 14 ($p < 0.05$). On the contrary, a significant reduction in the expression of the ACAN (0.76-fold, $p < 0.05$), Col II (0.68-fold, $p < 0.05$) and Sox-9 (0.43-fold, $p < 0.01$) was found in the Dex/Gel hydrogel on day 14 compared to that on day 7. Thus, the IPN hydrogel elicited a significant increase in the protein expression levels of ECM-related proteins compared to the PEG and Dex/Gel hydrogels on day 14. These results demonstrated that the IPN hydrogel could support the biosynthesis of the encapsulated NPCs and enhance the ECM secretion and deposition.

3.6. Phenotypical expression of chondrogenesis genes

Real-time PCR revealed differences in the chondrogenesis gene expression profiles for the NPCs cultured in the different scaffolds (Fig. 5K–M). ACAN, Col IIα1, and Sox-9 are important discogenic markers for NP, and they are essential to the matrix deposition and maintenance of the function of NPs. During the 14-day culture period, the expression levels of ACAN, Col IIα1, and Sox-9 increased continuously, and they were significantly higher in the IPN hydrogel compared to the PEG hydrogel ($p < 0.05$). On day 4, the expression levels of Col IIα1 and Sox-9 in the IPN hydrogel were less than that in the Dex/Gel hydrogel (0.35-fold and 0.37-fold,

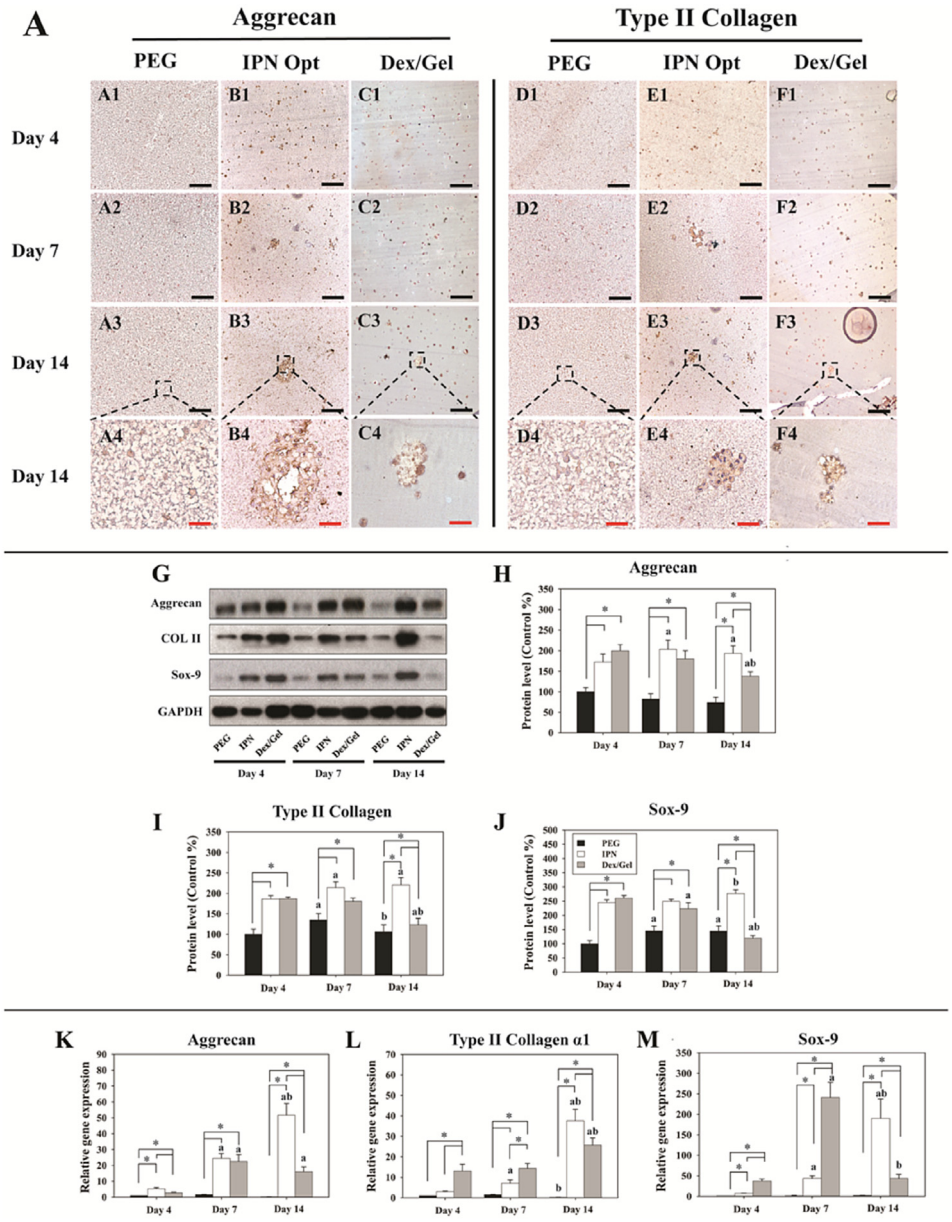

Fig. 5. ECM-related proteins and genes expression of the NPCs-encapsulated hydrogels. (A–C) The deposition of aggrecan in the NPCs-encapsulated (A1–A4) PEG hydrogels, (B1-B4) optimal IPN hydrogels and (C1-C4) Dex/Gel hydrogels. (n = 5). (D–F) The deposition of Col 2 in the NPCs-encapsulated (D1–D4) PEG hydrogels, (E1-E4) optimal IPN hydrogels and (F1-F4) Dex/Gel hydrogels. Black bar = 200 μm. Red bar = 50 μm. (n = 5). (G) Western blotting analysis of ECM proteins aggrecan, Col 2, Sox-9, produced by NPCs cultured in the cell-seeded PEG, optimal IPN and Dex/Gel hydrogels on day 4, 7 and 14. (H–J) The histogram of quantitative results of Western blotting analysis. Data were normalized to the data obtained from NPCs cultured in the PEG hydrogel on day 4 and evaluated on a relative basis for comparison between different samples. (K–M) The expressions of (K) aggrecan, (L) Col 2, (M) Sox-9 in the NPC-seeded PEG, optimal IPN, and Dex/Gel hydrogels on day 4,7 and 14. The expression levels, quantified using real-time PCR, are normalized to those of housekeeping gene, GADPH. Data are expressed as means ± SD. $^{a}p < 0.05$ for comparison with the same group on day 4, $^{b}p < 0.05$ for comparison with the same group on day 7. $^{*}p < 0.05$. (n = 3). (For interpretation of the references to colour in this figure legend, the reader is referred to the web version of this article.)

respectively, $p < 0.01$), while the ACAN expression was statistically similar ($p > 0.05$). On day 14, the expression levels of ACAN, Col IIα1 and Sox-9 genes within the IPN hydrogel were significantly up-regulated compared with the Dex/Gel hydrogel (3.23-fold, $p < 0.01$; 1.12-fold, $p < 0.05$; and 3.64-fold, $p < 0.01$, respectively). These results indicated that the NPCs encapsulated in the IPN Opt could maintain a normal chondrogenesis phenotype in the long term. Since the NPCs-IPN hydrogel hybrid exhibited a beneficial impact on NP regeneration, further animal experiments were performed with this group.

3.7. Biocompatibility of the hydrogels

To assess the fibrosis and inflammation of the surrounding tissue due to the gels, the IPN Opt, Dex/Gel, and PEG hydrogels were implanted in dorsal subcutaneous pockets in female Lewis rats for 8 weeks (Fig. 6). After 1 week, H&E staining showed that no granulocyte infiltration was observed around the embedded site for all the gel types, which demonstrates that the hydrogels did not cause an acute inflammatory response at the early implantation stage. Meanwhile, fibroblasts surrounded all the hydrogels, while the PEG and IPN hydrogels exhibited more fibroblast aggregation than the

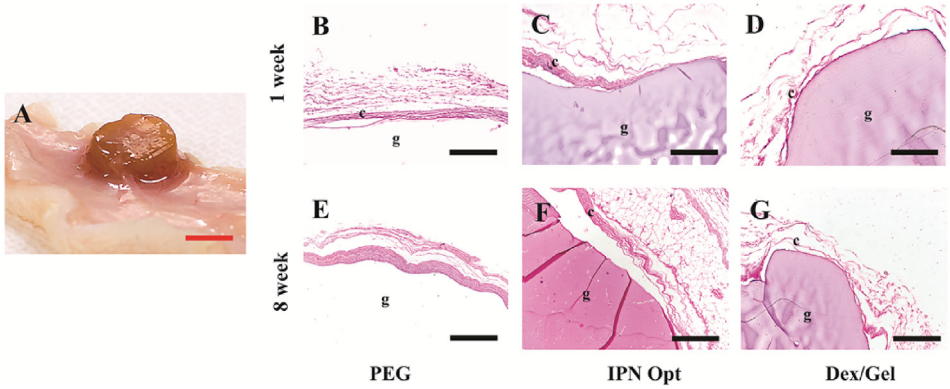

Fig. 6. Hydrogel implantation in rats subcutaneous. (A) View of the optimal IPN hydrogels encapsulated in a subcutaneous pocket at 8 weeks after implantation. (B–G) A representative overview of the encapsulated (B, E) PEG, (C, F) optimal IPN and (D, G) Dex/Gel hydrogels with the H&E staining at 1 and 8 weeks after implantation. Hydrogel location was labeled as "g". Collagen layer was labeled as "c". Red bar = 10 mm. Black bar = 200 μm. (n = 4). (For interpretation of the references to colour in this figure legend, the reader is referred to the web version of this article.)

Dex/Gel hydrogel (Fig. 6B-D). After 8 weeks, H&E staining showed the presence of a few macrophages or lymphocytic infiltrations for all the gel types, which illustrated a restricted chronic inflammatory response. After 8 weeks, a thin layer of fiber wrapping of the IPN Opt could be observed grossly (Fig. 6A). The encapsulated hydrogels resulted in a surrounding fibrotic collagen in all cases. However, the collagen condensation in the fibrotic sheath was thicker around the PEG hydrogel than the Dex/Gel and IPN hydrogel, which indicates a stronger response to the PEG hydrogel (Fig. 6E-G).

3.8. Cell and hydrogel retention in the rat IVD

To track the retention and survival of the encapsulated cells in the IPN hydrogel when they were implanted in the IVD *in vivo*, *in vivo* bioluminescent imaging was used after 4 weeks of injection of the cells-IPN hydrogel hybrid. The illuminating time was selected as 20 min based on the gelation efficiency test (Supplementary data 4). The total luminescence in a defined ROI was quantified before and after the 1 day and 28-day post-injection (Fig. 7). From day 1 to day 28 after the implantation, the total luminescence in the ROI was significantly higher (7.31-fold and 2.11-fold, respectively, $p < 0.01$) when the IPN hydrogel was used as the carrier for cell delivery than that when PBS was used as the carrier, which indicates a high cell retention and survival in the IPN. Although the bioluminescent signal decayed at 28-day post-implantation compared with that at day 1 in the IPN hydrogel (0.30-fold, $p < 0.01$), the NPCs-luc were almost limited to the NP cavity (Fig. 7B). In contrast, the NPCs-luc delivered with PBS escaped from the IVD and survived in the whole body. Few living NPCs-luc existed in the rat in the PBS group on day 28 because of the host response to ectopic cells (Fig. 7D).

3.9. Rehydration and height maintenance of the porcine IVD after the hydrogel implantation in vivo

To explore the rehydration effect after the IPN hydrogel injection, MRI analysis was used to quantify the hydration of the IVD (Fig. 8A, B1-B4, D). After 1-day post-injection, there was no significant difference in the intensity of the T2-weighted signal among the IVDs in all groups ($p > 0.05$). As the regenerative time increased, the IVD exhibited an obvious degenerative sign of the decayed T2-weighted signal with PBS as the cell carrier. In contrast, the cell-seeded IPN hydrogel resulted in an elevated intensity of the T2-weighted signal at the time points of 3 and 6 weeks compared to the PBS- and gel-only groups ($p < 0.01$). After 12-weeks post-injection, the intensity was higher in the IVD with the implanted

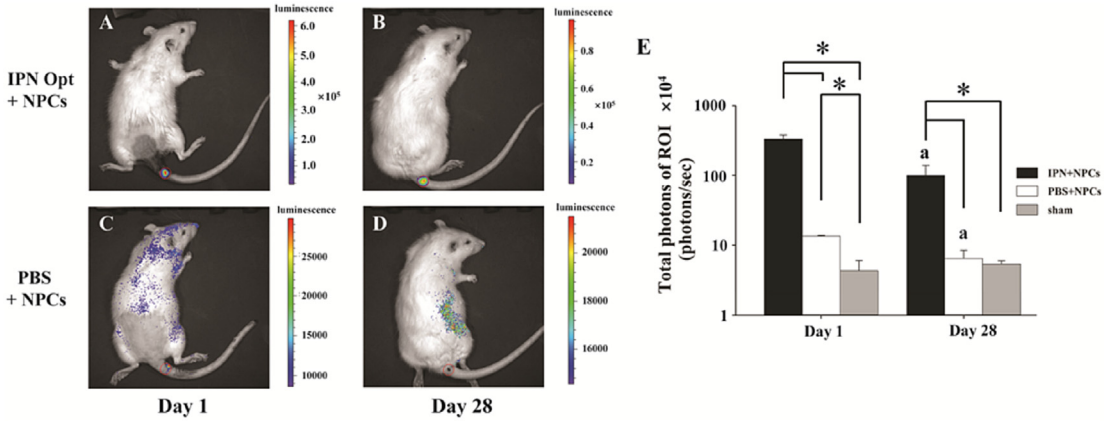

Fig. 7. Cell retention in IVDs of rat tail. (A–D) NPCs-luc were delivered to IVDs of rat rail using (A, C) optimal IPN hydrogel or (B, D) PBS as carriers at 1 day and 28 days post cell injection. Cell retention was measured by total luminescence per motion segment. (E) The histogram of total luminescence per motion segment in the region of interest (ROI) in overlay images. ROI was represented by a red circle. Data are expressed as means ± SD. *$p < 0.05$. [a]$p < 0.05$ for comparison with the same group on day 1. (n = 5). (For interpretation of the references to colour in this figure legend, the reader is referred to the web version of this article.)

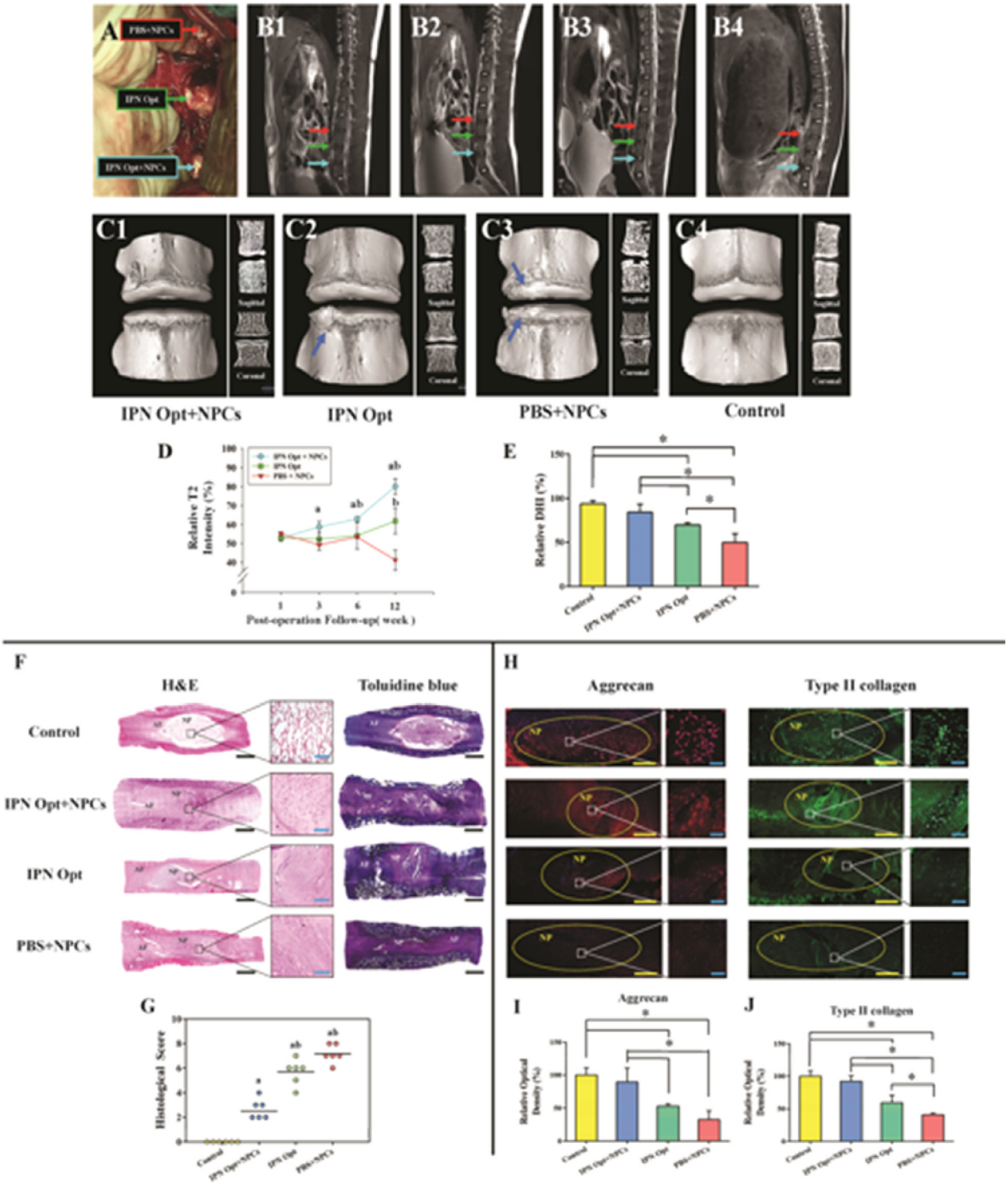

Fig. 8. *In vivo* study of the regenerative effect of the IPN hydrogel in porcine disc degeneration model. (A) Exposure of target porcine IVDs prepared for implanting NPCs-seeded PBS (red arrow), optimal IPN hydrogels only (green arrow) or NPCs-seeded optimal IPN hydrogel (blue arrow) in operation. (B) Representative images of MRI scanning for porcine at 1 week, 3 weeks, 6 weeks and 12 weeks after implantation. (C) Representative images of micro-CT reconstructions obtained from the (C1) L2–L3, (C2) L3-L4, (C3) L4-L5, and (C4) L1-L2 level from operated porcine at 12 weeks. The degenerative osteophytes were indicated with a blue arrow. (D) Plots of T2-weighted signal intensity from MRI scanning in each group at 1 week, 3 weeks, 6 weeks and 12 weeks after implantation. $^{a}p < 0.05$ for comparison with the IPN Opt group at the same time point, $^{b}p < 0.05$ for comparison with the PBS + NPCs group at same time point. (E) Relative DHI of each group at 12 weeks after implantation. (F) Representative H&E and toluidine blue staining of the tissue at 6 weeks. Different regions (NP and AF) were indicated in the tissue sections. (G) Histological scores were obtained from each group at 12 weeks after implantation. $^{a}p < 0.05$ for comparison with the Control group, $^{b}p < 0.05$ for comparison with the IPN Opt + NPCs group. (H) Immunofluorescence observation of aggrecan and type II collagen in NP tissues from each group at 12 weeks after implantation. ROIs (NP) were indicated in the image. (I–J) Quantitative examination of the immunofluorescence analysis. Black bar = 2000 μm. Blue bar = 100 μm. Yellow bar = 1000 μm. Data are expressed as means ± SD. $^{*}p < 0.05$. (n = 3). (For interpretation of the references to colour in this figure legend, the reader is referred to the web version of this article.)

Table 3
Description of the degenerate degree in the operated discs considering structure, MRI signal intensity and intervertebral height by Pfirmann classification.

Follow-up period	Pfirmann Classification for each disc				
	animal	L1-L2(control)	L2-L3(PBS + NPCs)	L3-L4(IPN)	L4-L5(IPN + NPCs)
1 week follow-up postoperatively	1	I	IV	IV	IV
	2	I	V	IV	IV
	3	I	IV	IV	V
3 week follow-up postoperatively	1	I	IV	IV	III
	2	I	V	V	IV
	3	I	V	IV	IV
6 week follow-up postoperatively	1	I	IV	III	III
	2	II	V	IV	III
	3	I	V	IV	III
12 week follow-up postoperatively	1	I	V	III	III
	2	II	V	III	II
	3	I	V	IV	II

cell-seed IPN hydrogel than the IPN hydrogel alone ($p < 0.05$) and the cell-seed PBS ($p < 0.01$), although its intensity was significantly lower than that in the control group (data not shown). The results illustrated a favorable IVD rehydration effect from the strategy of IPN-based TE-NP implantation.

The DHI is a crucial indicator to evaluate disc degeneration, which was calculated from the micro-CT evaluation. As shown in Fig. 8C1-4 and E, the relative DHI remained significantly higher in the cell-seeded IPN hydrogel than the IPN hydrogel-only group ($p < 0.05$) and the cell-PBS group ($p < 0.01$) at 12 weeks after the operation. Moreover, there were definite degenerate osteophytes in the IPN hydrogel-only group and the cell-PBS group (blue arrows). In contrast, there no osteophytes were found in the cell-seeded IPN hydrogel group. This result demonstrated that the height of the intervertebral space could be maintained close to a healthy one, and the degenerative degree of the IVD could be alleviated when it is injected with the cell-seeded IPN hydrogel.

The sagittal sections of the operated IVDs were indicated with H&E and toluidine blue staining (Fig. 8F). The structure of the IVD implanted with a cells-IPN hybrid was much homogeneous than that of IPN only group and cells-PBS group. It illustrated that the IPN Opt could play a positive role as a regenerative template for NP in long-term implantation. The NP region in the cells-IPN hybrids implantation group was not as much hydrated as the control group, but this should attribute to the relatively short follow-up duration and longer degradation time of the high crosslinked density of the IPN hydrogel. Histological grading showed that the mean score of the cell-IPN hydrogel group was significantly lower than that of the IPN hydrogel-only group ($p < 0.05$) and cell-PBS group ($p < 0.01$) at 8 weeks (Fig. 8G), also demonstrating the much lower degeneration degree when using the IPN Opt as the NPCs' carrier. The results of Pfirmann classification is in agreement with the superior outcomes (Table 3). Additionally, the immunofluorescence results (Fig. 8H) and the associated quantitative analysis (Fig. 8I and J) showed that the expressions of ACAN and Col II in the cell-IPN hydrogel group were up-regulated compared to those of the IPN hydrogel-only group ($p < 0.05$) and cell-PBS group ($p < 0.05$) throughout the NP region.

4. Discussion

Owing to the accelerated aging population, therapy for IDD has been widely considered in recent years. Cell-based biological therapy for IDD may be better suitable to alleviate pain, repair degenerative NP and further restore the biomechanical function of the IVD than traditional treatments. However, it is still challenging to find appropriate scaffolds and delivery strategies. A hydrogel as a proper NP scaffold should not only support cell growth and matrix deposition but should also exhibit enough mechanical strength to provide a powerful template for spatial and temporal NP regeneration. Meanwhile, the injectable property of the hydrogel should also be considered as a priority to avoid aggravating the AF injury. In this study, a mechanically tunable IPN was applied to achieve these requirements. The aim was to realize IVD regeneration using the IPN hydrogel-based TE-NP in large animal models. Therefore, we optimize mechanical properties, evaluate the symmetrical physical and biological properties of the IPN for NP regeneration and determine the preparation conditions that are most suitable for NP regeneration. To our knowledge, this is the first study that evaluates the feasibility of the IPN hydrogel as a scaffold for NP regeneration systematically and applies it to repair the IVD *in situ* and *in vivo*.

4.1. Optimal mechanical properties of the hydrogel for TE-NP

A number of previous studies focused on Young's modulus and shear modulus when adjusting the mechanical properties of the NP scaffold and made progress to match the properties to that of the NP tissue [36,51]. In addition to these parameters, the toughness should also be emphasized as another essential criterion of the hydrogel scaffold. The non-degenerative NP is a soft, viscous tissue, which cannot independently resist the compression. When the NP is restricted by the surrounding AF and CEPs, the composite becomes a strong mechanical buffer by the high intradiscal pressure that originates from the compression-induced fluid flow and lateral expansion [13]. Thus, fluid pressurization is the primary mechanical function of the NP. Nevertheless, the integrity of the IVD was damaged when tears that appear in the AF cause the NP to bulge out, which is common in a patient with advanced DDD. Thus, the IVD loses the capability to absorb the compression. Moreover, the destruction of the facets of the lumbar spine leads to increasing compressive load of the IVD during the disc degeneration. Therefore, the high toughness of the scaffold benefits the preservation of the original 3D environment during repeated deformation and improves the resilience under the cyclically severe compression in the NP cavity [28]. Also, the high toughness of the hydrogel scaffold helps the retention of the implant in the implantation site, which promotes the long-term biological effect of regeneration.

The mass ratio of the second network to the first network was tuned to achieve high toughness, NP-like stiffness and shear modulus of the hydrogels. The IPN hydrogel at the optimal ratio of 1:4 exhibited ideal mechanical properties with an extremely high toughness. The stiffness and toughness of the IPN hydrogels can be explained from three aspects. First, the highly crosslinked PEG networks exhibited high Young's modulus but brittleness to sustain compression; they act as the skeleton of the IPN hydrogel, which

ascribes the hydrogel with dominating stiffness. Second, the reinforcement effect is provided by the incorporation of the Dex/Gel network, which is, in contrast, soft and relatively ductile. The high toughness might be achieved by an efficient energy dispersion under deformation by the loosely crosslinked networks of Dex/Gel, which enhances the possibility of the resistance to the hydrogel. Lastly, we combined the dual networks at a reasonable ratio of the lower-concentration relatively rigid, brittle networks interpenetrated with the higher concentration softer, more ductile network to realize the synergistic mechanism of a substantial improvement in the mechanical performance, which was reported by a previous study [35,52]. Because neither of the networks individually satisfies the mechanical requirement of TE-NP, the rational combination in this study would bring the synergistic mechanism of the hydrogel, resulting in an effortless deformation but no rupture under the cyclic compression.

For the bionics aspect, the interpenetrating structure is the basis of compression buffering of the IPN hydrogel. In the native NP, the network of the Col II forms the skeleton and provides the original mechanical properties of the NP. The proteoglycans are embedded within collagen fibrils in the network and are responsible for much of the water-retaining properties through the attached sulfated GAG. The interpenetrating networks of the IPN hydrogel accurately mimicked the microstructure of the ECM of the native NP, where the PEG networks act as the primary frame structure and the ODex-MGel networks act as fillers in the skeleton, as shown in the histological result.

The viscoelastic properties are another important characteristic for the clinical application of hydrogels. The stiffness or the resistance to dynamic conditions of the hydrogel can be illustrated by $|G^*|$, while the dissipation under shearing can be exhibited by δ. The $|G^*|$ value of the optimal IPN hydrogel is in the range 7–21 kPa of the native NP tissue [53] over the range of frequencies from 1 to 100 rad s^{-1}, indicating a similar resistance capability of dynamic shearing as the NP tissue. However, the much smaller δ value of the IPN hydrogel than NP (23–31°) demonstrated that the elastic behavior of the hydrogel is dominant, which is conducive to prevent it from bulging out from the NP cavity.

The state of hydration of the NP is an important determinant of the mechanical behavior in the IVD. The load-bearing ability of the NP is more dependent on internal hydrostatic pressure than the elastic modulus [53]. The constant diurnal fluctuations of the compression lead to this pumping effect of fluid movement into and out of the disc matrix [54]. The balance between external loading and NP hydration is key to the maintenance of the IVD height. The hydration of the optimal IPN hydrogel was close to that of the native NP under high compression, which is favorable to the mechanical support as an NP implant.

In this study, the optimal mechanical properties were obtained at a ratio of 1:4 of the secondary network to the primary network. An increasing proportion of the second network could not result in further improvements in the toughness. Therefore, more work is required to clarify the toughening mechanisms of the IPN hydrogel.

4.2. Cytocompatibility and ECM deposition of encapsulated NPCs in the IPN hydrogel

Cell clustering is regarded as an important capability of juvenile NPCs [55]. It has been reported that the enhanced cell-cell interaction associated with cell clustering behavior is benign for chondrogenesis and potentially helpful for the maturation of engineered constructs [56,57]. Upon degeneration, the NPCs lose their capability for cell-cell interactions and form a limited amount of small, chondrocyte-like cells [58]. Previous studies have reported that hydrogels with higher crosslinking density limit the size of cell clusters because cell movement is restricted by the small mesh size [59]. In this study, the mechanically stronger IPN hydrogels have a small initial mesh size in the range of 4–8 nm owing to the relatively higher crosslink density. However, the size of the cell clusters with a chondrocyte-like round morphology increased as the culture period in the IPN hydrogel increased. This should attribute adhesive properties and a rapid degradation of the natural network of Dex/Gel to the cell. It could support the adhesion of NPCs in the early period while providing the macropore space for cell proliferation in the later period. In contrast, the Dex/Gel network alone would collapse after 14-days post-seeding, which would make it unable to support the discogenesis. The mechanical stability could be enhanced by interpenetrating with the synthetic network of PEG, which provides a long-term 3D template for tissue formation. However, the NPCs in the pure PEG hydrogel existed as single cells or small isogenous cell clusters with the morphology of cell shrinkage, as in the aging NP, which is a fundamental feature of apoptosis. Although neither of the two networks alone could support long-term cell survival in the implant, the synergistic effect of them is particularly suitable for neo-NP tissue formation.

A favorable 3D culture environment could also promote the viability of the NPCs and maintain their phenotypic characteristics [60]. The live cell percentage was above 95%, while the DNA content was constantly elevated in the IPN hydrogel. The plausible explanation for this is that the nutrition diffusion increased with the degradation of Dex/Gel [61]. The expression of biosynthesis-related genes was up-regulated in the IPN hydrogel than the PEG and Dex/Gel hydrogels after 2 weeks. The gradually increasing cell viability and biosynthesis genes expression were probably because the encapsulated NPCs adapted to the 3D environment of the IPN hydrogel and functioned properly after the culture period. These results demonstrated that the formulations of the IPN hydrogel used in this study appeared to be suitable for the maintenance of a chondrogenesis phenotype and the promotion of the elaboration of a proper ECM.

The hierarchical structure of the IPN hydrogel is also beneficial for spatial ECM distribution. In accordance with previous studies, the small mesh size of the hydrogel with high crosslinking density hinders the matrix elaboration, as evidenced by the fact that the ACAN and Col II were confined intracellularly in the PEG hydrogel. The deposition of these cartilage-specific ECM, on the contrary, were increased in the IPN hydrogel with the extension of the culture time, which was proven by the Western Blotting results, and the ECM aggregated in the pericellular region, as observed in the immunohistochemical results. On one hand, cell clustering could promote ECM deposition with the increasing inner space due to the Dex/Gel network degradation. On the other hand, the ECM expression could also be enhanced by the high cell viability of encapsulated NPCs. Additionally, the higher water content allows an increased diffusion of nutrients into the hydrogel. It is noteworthy that the toluidine blue-stained sulfated GAG could be uniformly diffused in the IPN hydrogel, which indicated that the distribution of the macromolecules with relatively low molecular weight allowed their transportation in the hydrogel.

4.3. Biocompatibility and long-term regenerative effect in vivo

The foreign body reaction *in vivo* should be considered when the hydrogel is used for implant application with a high degree of the hydrogel-body interaction. The dorsal implantation study suggests a minimal inflammation of the IPN hydrogels *in vivo*. The results demonstrated an absence of immune cells and a mild fibrotic response caused by all the hydrogel types. These results agree with the study of the favorable *in vivo* biocompatibility of the Dex/Gel hydrogel [62] and PEG hydrogel [63]. The comparable histological

response among the IPN, Dex/Gel, and PEG hydrogels indicated the non-inflammatory nature of the IPN hydrogels.

The pressure-induced extrusion in IVD is a challenge in the application of an injected material. The superior properties of the photopolymerizable IPN hydrogel in this study are quite suitable for the requirements of scaffolds for NP regeneration [64]. The injected precursor could immerse into the microroughness of the surrounding tissue, leading to beneficial tissue integration after polymerization. In addition, it improves the tissue/implant interface and subsequently results in the formation of mechanical interlocking [65,66], thus providing reliable biological fixation, reducing the danger of heterotopic grafting, and facilitating the healing process [67]. To visualize the process and implant retention *in vivo*, the small animal model was observed for 4 weeks after the NPCs-luc-IPN hydrogel hybrid implantation, as described by Francisco et al. [68]. As expected, the photocrosslinking hydrogel significantly improved cell retention and survival when compared to the PBS. Although only 30% of the bioluminescent signal intensity remained in the IVD after 4 weeks, this should attribute to the thick needle for injection and light guide. Even so, the retention result was significantly improved than the previous study, which should be attributed to the tough, ductile and photocurable characteristics of the IPN hydrogel. The positive result indicates that the implanted IPN hydrogel could be sustained in the IVD under a high intradiscal pressure in the long term.

Due to the difference between the structure and function of the small animal and human IVD, the regenerative effect of the IVD with implanted cell-based IPN hydrogel should be verified in the large animal model. The porcine IVD is known to share similar characteristics with the human IVD [69,70]. Therefore, the porcine disc degeneration model was used to simulate the repairing effect in humans. As our hypothesis, the tough IPN hydrogel could provide a long-term template for NP regeneration, demonstrated by the significantly higher rehydration and ECM deposition in the IVD injected with the NPCs-seeded IPN hydrogel after 3 months' post-implantation. Meanwhile, the DHI was also significantly higher, and no degenerative osteophyte formation was observed in the cell-seeded IPN hydrogel group. Although the rehydration effect is still inferior to natural NP, expanding follow-up period is possible to achieve a better result for more hydrogel degradation and natural matrix synthesis. Because the NP region was completely emptied before transplanting, these positive results provide a powerful evidence of neo-NP tissue formation, which subsequently results in repair of the degenerative IVD. We believe that the toughness of the scaffold should be considered as a priority for regenerating late-stage disc degeneration and disc herniation. This is different from some previous studies, which placed emphasis on the bioactivities of hydrogels for the treatment of early-stage disc degeneration [36,71]. The distinction is because the implant easily bulged out through large AF fissures under compression in the late-stage disc degeneration and disc herniation. The tough IPN hydrogel in the study provides satisfactory compression resistance, which is observed in both the *in vitro* and *in vivo* study. Therefore, our study demonstrated that the IPN hydrogel is a potential choice for further disc regeneration.

There are some limitations to this study. Firstly, an optical fiber was used to guide the UV into the NP cavity. For the *in vivo* study, it is inaccurate to estimate photopolymerization efficiency of the optical fiber *in vitro*. It is important to note that Schmocker et al. recently reported a novel minimally invasive device for photopolymerized hydrogels *in situ*, which can monitor the entire curing volume [72,73]. The device is ideal for the photopolymerization of hydrogel in NP. Secondly, a smaller optical fiber and an illuminating laser would be needed in the future to use 25G or 26 G needle as guidance to prevent disc injury and implant leakage [74,75]. Thirdly, the disc degeneration model here exhibited several inevitable drawbacks. It was not equal to the complex pathological process of human disc degeneration. In particular, the late-stage degenerative state of the AF could not be precisely simulated in the model. Previous study indicated the nucleotomy would develop to disc degeneration in 3 weeks [45]. In this study, the discs were repaired immediately after nucleotomy to prevent the generation of the scar fibrotic tissue which would hinder the gel injection, possibly decreasing clinical relevance of the model. Meanwhile, the influence of adjacent disc degeneration can't be avoided when all groups were adjacent to each other even though the effect was relatively little in reptiles with less influence of gravity on the disc. In addition, the load-bearing of the IVD in reptiles is smaller than that of humans. However, the porcine disc degeneration model here is still an alternative choice for studying the disc regeneration strategy under the harsh mechanical environment of late-stage disc degeneration on the condition of the scarcity of standing animals, even if it has these defects. The reason is the IVD still bears a much higher loading on the IVD induced by dorsal muscle contraction of large animals than small animals. For further research, the model should be improved to reduce its defects as much as possible. Fourthly, it is unknown whether IPN hydrogel could maintain the NP-specific phenotype of encapsulated NPCs, which has a critical influence on NP regeneration and should be explored deeply. Finally, the tough IPN hydrogel could support NP regeneration in the long-term *in vivo* study, exhibiting the possibilities of restoring the function of IVD using the gel. In order to realize the functional regeneration of NP using the gel, more functional parameters should be focused in the future study. In summary, the IPN hydrogel in this study can realize a better regenerative effect, which is promising to be converted to clinical application in the future.

5. Conclusions

In this study, an IPN-strengthened and toughened hydrogel was developed for regeneration of NP. The optimal formulation of the IPN hydrogel at a ratio of 1:4 showed various potential advantages including NP-like mechanical properties and high toughness. The tough and ductile characteristics of the IPN hydrogel provide a long-term regenerative template for NP regeneration under the compression and resistance to pressure-induced extrusion. The encapsulated NPCs exhibited improved proliferation, a native chondrogenesis phenotype and increased ECM secretion in the IPN hydrogels. Furthermore, our *in vivo* study showed that the IPN hydrogel supports long-term cell retention and survival while facilitating rehydration and regeneration of degenerative NPs. These results demonstrate that the IPN hydrogel can be applied as a promising NP scaffold for regenerating late-stage disc degeneration.

Conflict of interest statement

There is no conflict of interest.

Acknowledgments

This study was supported by the NSFC (grant number 81272029); the NSFC (grant number 81027005); the Transformation of Scientific and Technological Achievements of the Third Military Medical University (grant number 2011XZH006); and Key Project of Military Logistics (grant number BWS13C014-1). The authors thank Yujie Hua, Xiaohua Geng and Xi Wang for excellent technical support.

Appendix A. Supplementary data

Supplementary data related to this article can be found at http://dx.doi.org/10.1016/j.biomaterials.2017.05.017.

References

[1] M. Juniper, T.K. Le, D. Mladsi, The epidemiology, economic burden, and pharmacological treatment of chronic low back pain in France, Germany, Italy, Spain and the UK: a literature-based review, Expert Opin. Pharmacother. 10 (2009) 2581–2592, http://dx.doi.org/10.1517/14656560903304063.

[2] F. Pellise, F. Balague, L. Rajmil, C. Cedraschi, M. Aguirre, C.G. Fontecha, et al., Prevalence of low back pain and its effect on health-related quality of life in adolescents, Arch. Pediatr. Adolesc. Med. 163 (2009) 65–71, http://dx.doi.org/10.1001/archpediatrics.2008.512.

[3] A. Di Martino, A.R. Vaccaro, J.Y. Lee, V. Denaro, M.R. Lim, Nucleus pulposus replacement: basic science and indications for clinical use, Spine 30 (2005) S16–S22.

[4] M.D. Humzah, R.W. Soames, Human intervertebral disc: structure and function, Anat. Rec. 220 (1988) 337–356, http://dx.doi.org/10.1002/ar.1092200402.

[5] W. Johannessen, D.M. Elliott, Effects of degeneration on the biphasic material properties of human nucleus pulposus in confined compression, Spine 30 (2005) E724–E729.

[6] A. Bailey, A. Araghi, S. Blumenthal, G.V. Huffmon, Anular repair clinical study G. prospective, multicenter, randomized, controlled study of anular repair in lumbar discectomy: two-year follow-up, Spine 38 (2013) 1161–1169, http://dx.doi.org/10.1097/BRS.0b013e31828b2e2f.

[7] F. Heuer, S. Ulrich, L. Claes, H.J. Wilke, Biomechanical evaluation of conventional anulus fibrosus closure methods required for nucleus replacement, Laboratory investigation, J. Neurosurg. Spine 9 (2008) 307–313, http://dx.doi.org/10.3171/SPI/2008/9/9/307.

[8] H. Brisby, Pathology and possible mechanisms of nervous system response to disc degeneration, J. Bone Jt. Surg. Am. 88 (Suppl 2) (2006) 68–71, http://dx.doi.org/10.2106/JBJS.E.01282.

[9] S. Roberts, H. Evans, J. Trivedi, J. Menage, Histology and pathology of the human intervertebral disc, J. Bone Jt. Surg. Am. 88 (Suppl 2) (2006) 10–14, http://dx.doi.org/10.2106/JBJS.F.00019.

[10] G. Leivseth, R. Salvesen, S. Hemminghytt, P. Brinckmann, W. Frobin, Do human lumbar discs reconstitute after chemonucleolysis? A 7-year follow-up study, Spine 24 (1999) 342–347 discussion 8.

[11] H.A. Horner, J.P. Urban, Volvo award winner in basic science studies: effect of nutrient supply on the viability of cells from the nucleus pulposus of the intervertebral disc, Spine 26 (2001) 2543–2549.

[12] J. Silva-Correia, S.I. Correia, J.M. Oliveira, R.L. Reis, Tissue engineering strategies applied in the regeneration of the human intervertebral disk, Biotechnol. Adv. 31 (2013) 1514–1531, http://dx.doi.org/10.1016/j.biotechadv.2013.07.010.

[13] J.C. Iatridis, S.B. Nicoll, A.J. Michalek, B.A. Walter, M.S. Gupta, Role of biomechanics in intervertebral disc degeneration and regenerative therapies: what needs repairing in the disc and what are promising biomaterials for its repair? Spine J. Off. J. North Am. Spine Soc. 13 (2013) 243–262, http://dx.doi.org/10.1016/j.spinee.2012.12.002.

[14] J. Silva-Correia, A. Gloria, M.B. Oliveira, J.F. Mano, J.M. Oliveira, L. Ambrosio, et al., Rheological and mechanical properties of acellular and cell-laden methacrylated gellan gum hydrogels, J. Biomed. Mater. Res. Part A 101 (2013) 3438–3446, http://dx.doi.org/10.1002/jbm.a.34650.

[15] A.S. Hoffman, Hydrogels for biomedical applications, Adv. drug Deliv. Rev. 54 (2002) 3–12.

[16] A.I. Chou, S.O. Akintoye, S.B. Nicoll, Photo-crosslinked alginate hydrogels support enhanced matrix accumulation by nucleus pulposus cells in vivo, Osteoarthr. Cartil./OARS, Osteoarthr. Res. Soc. 17 (2009) 1377–1384, http://dx.doi.org/10.1016/j.joca.2009.04.012.

[17] Z. Sun, B. Luo, Z. Liu, L. Huang, B. Liu, T. Ma, et al., Effect of perfluorotributylamine-enriched alginate on nucleus pulposus cell: implications for intervertebral disc regeneration, Biomaterials 82 (2016) 34–47, http://dx.doi.org/10.1016/j.biomaterials.2015.12.013.

[18] A. Di Martino, M. Sittinger, M.V. Risbud, Chitosan: a versatile biopolymer for orthopaedic tissue-engineering, Biomaterials 26 (2005) 5983–5990, http://dx.doi.org/10.1016/j.biomaterials.2005.03.016.

[19] P. Roughley, C. Hoemann, E. DesRosiers, F. Mwale, J. Antoniou, M. Alini, The potential of chitosan-based gels containing intervertebral disc cells for nucleus pulposus supplementation, Biomaterials 27 (2006) 388–396, http://dx.doi.org/10.1016/j.biomaterials.2005.06.037.

[20] D. Sakai, J. Mochida, Y. Yamamoto, T. Nomura, M. Okuma, K. Nishimura, et al., Transplantation of mesenchymal stem cells embedded in Atelocollagen gel to the intervertebral disc: a potential therapeutic model for disc degeneration, Biomaterials 24 (2003) 3531–3541.

[21] E.C. Collin, S. Grad, D.I. Zeugolis, C.S. Vinatier, J.R. Clouet, J.J. Guicheux, et al., An injectable vehicle for nucleus pulposus cell-based therapy, Biomaterials 32 (2011) 2862–2870, http://dx.doi.org/10.1016/j.biomaterials.2011.01.018.

[22] D.R. Pereira, J. Silva-Correia, S.G. Caridade, J.T. Oliveira, R.A. Sousa, A.J. Salgado, et al., Development of gellan gum-based microparticles/hydrogel matrices for application in the intervertebral disc regeneration, Tissue Eng. Part C. Methods 17 (2011) 961–972, http://dx.doi.org/10.1089/ten.TEC.2011.0115.

[23] J. Silva-Correia, V. Miranda-Goncalves, A.J. Salgado, N. Sousa, J.M. Oliveira, R.M. Reis, et al., Angiogenic potential of gellan-gum-based hydrogels for application in nucleus pulposus regeneration: in vivo study, Tissue Eng. Part A 18 (2012) 1203–1212, http://dx.doi.org/10.1089/ten.TEA.2011.0632.

[24] Y.H. Cheng, S.H. Yang, W.Y. Su, Y.C. Chen, K.C. Yang, W.T.K. Cheng, et al., Thermosensitive chitosan-gelatin-glycerol phosphate hydrogels as a cell carrier for nucleus pulposus regeneration: an in vitro study, Tissue Eng. Pt A 16 (2010) 695–703, http://dx.doi.org/10.1089/ten.tea.2009.0229.

[25] W.Y. Su, Y.C. Chen, F.H. Lin, Injectable oxidized hyaluronic acid/adipic acid dihydrazide hydrogel for nucleus pulposus regeneration, Acta Biomater. 6 (2010) 3044–3055, http://dx.doi.org/10.1016/j.actbio.2010.02.037.

[26] S.H. Park, H. Cho, E.S. Gil, B.B. Mandal, B.H. Min, D.L. Kaplan, Silk-fibrin/hyaluronic acid composite gels for nucleus pulposus tissue regeneration, Tissue Eng. Part A 17 (2011) 2999–3009, http://dx.doi.org/10.1089/ten.TEA.2010.0747.

[27] S.C. Chan, B. Gantenbein-Ritter, Intervertebral disc regeneration or repair with biomaterials and stem cell therapy–feasible or fiction? Schweiz. Med. Wochenschr. 142 (2012) 1606–1610.

[28] N. Tanaka, H.S. An, T.H. Lim, A. Fujiwara, C.H. Jeon, V.M. Haughton, The relationship between disc degeneration and flexibility of the lumbar spine ☆, Spine J. 1 (2001) 47–56.

[29] H. Mizuno, A.K. Roy, V. Zaporojan, C.A. Vacanti, M. Ueda, L.J. Bonassar, Biomechanical and biochemical characterization of composite tissue-engineered intervertebral discs, Biomaterials 27 (2006) 362–370, http://dx.doi.org/10.1016/j.biomaterials.2005.06.042.

[30] X. Geng, X. Mo, L. Fan, A. Yin, J. Fang, Hierarchically designed injectable hydrogel from oxidized dextran, amino gelatin and 4-arm poly (ethylene glycol)-acrylate for tissue engineering application, J. Mater. Chem. 22 (2012) 25130–25139.

[31] S. Stern, K. Lindenhayn, O. Schultz, C. Perka, Cultivation of porcine cells from the nucleus pulposus in a fibrin/hyaluronic acid matrix, Acta Orthop. Scand. 71 (2000) 496–502, http://dx.doi.org/10.1080/000164700317381207.

[32] X. Mo, H. Iwata, S. Matsuda, Y. Ikada, Soft tissue adhesive composed of modified gelatin and polysaccharides, J. Biomater. Sci. Polym. Ed. 11 (2000) 341–351.

[33] S.T. Li, Y. Liu, Q. Zhou, R.F. Lue, L. Song, S.W. Dong, et al., A novel axial-stress bioreactor system combined with a substance exchanger for tissue engineering of 3D constructs, Tissue Eng. Part C. Methods 20 (2014) 205–214, http://dx.doi.org/10.1089/ten.TEC.2013.0173.

[34] S.P. Grogan, S. Sovani, C. Pauli, J. Chen, A. Hartmann, C.W. Colwell Jr., et al., Effects of perfusion and dynamic loading on human neocartilage formation in alginate hydrogels, Tissue Eng. Part A 18 (2012) 1784–1792, http://dx.doi.org/10.1089/ten.TEA.2011.0506.

[35] L. Wang, G. Shan, P. Pan, A strong and tough interpenetrating network hydrogel with ultrahigh compression resistance, Soft Matter 10 (2014) 3850–3856, http://dx.doi.org/10.1039/c4sm00206g.

[36] Y.C. Chen, W.Y. Su, S.H. Yang, A. Gefen, F.H. Lin, In situ forming hydrogels composed of oxidized high molecular weight hyaluronic acid and gelatin for nucleus pulposus regeneration, Acta Biomater. 9 (2013) 5181–5193, http://dx.doi.org/10.1016/j.actbio.2012.09.039.

[37] P.B. Welzel, S. Prokoph, A. Zieris, M. Grimmer, S. Zschoche, U. Freudenberg, et al., Modulating biofunctional starPEG heparin hydrogels by varying size and ratio of the constituents, Polymers 3 (2011) 602–620.

[38] S.S. Sivan, S. Roberts, J.P. Urban, J. Menage, J. Bramhill, D. Campbell, et al., Injectable hydrogels with high fixed charge density and swelling pressure for nucleus pulposus repair: biomimetic glycosaminoglycan analogues, Acta Biomater. 10 (2014) 1124–1133, http://dx.doi.org/10.1016/j.actbio.2013.11.010.

[39] V.A. Parsegian, R.P. Rand, N.L. Fuller, D.C. Rau, Osmotic stress for the direct measurement of intermolecular forces, Methods Enzym. 127 (1986) 400–416.

[40] J.P. Urban, J.F. McMullin, Swelling pressure of the lumbar intervertebral discs: influence of age, spinal level, composition, and degeneration, Spine 13 (1988) 179–187.

[41] B.J. DeKosky, N.H. Dormer, G.C. Ingavle, C.H. Roatch, J. Lomakin, M.S. Detamore, et al., Hierarchically designed agarose and poly(ethylene glycol) interpenetrating network hydrogels for cartilage tissue engineering, Tissue Eng. Part C. Methods 16 (2010) 1533–1542, http://dx.doi.org/10.1089/ten.tec.2009.0761.

[42] N. Blumenkrantz, G. Asboe-Hansen, An assay for hydroxyproline and proline on one sample and a simplified method for hydroxyproline, Anal. Biochem. 63 (1975) 331–340.

[43] Y. Nagai, H. Yokoi, K. Kaihara, K. Naruse, The mechanical stimulation of cells in 3D culture within a self-assembling peptide hydrogel, Biomaterials 33 (2012) 1044–1051, http://dx.doi.org/10.1016/j.biomaterials.2011.10.049.

[44] A.T. Francisco, R.J. Mancino, R.D. Bowles, J.M. Brunger, D.M. Tainter, Y.T. Chen, et al., Injectable laminin-functionalized hydrogel for nucleus pulposus regeneration, Biomaterials 34 (2013) 7381–7388.

[45] G.W. Omlor, A.G. Nerlich, H.J. Wilke, M. Pfeiffer, H. Lorenz, M. Schaaf-Keim, et al., A new porcine in vivo animal model of disc degeneration: response of anulus fibrosus cells, chondrocyte-like nucleus pulposus cells, and notochordal nucleus pulposus cells to partial nucleotomy, Spine 34 (2009) 2730–2739, http://dx.doi.org/10.1097/BRS.0b013e3181b723c9.

[46] C.W. Pfirrmann, A. Metzdorf, M. Zanetti, J. Hodler, N. Boos, Magnetic

resonance classification of lumbar intervertebral disc degeneration, Spine 26 (2001) 1873–1878.
[47] F. Yang, V.Y. Leung, K.D. Luk, D. Chan, K.M. Cheung, Mesenchymal stem cells arrest intervertebral disc degeneration through chondrocytic differentiation and stimulation of endogenous cells, Mol. Ther. : J. Am. Soc. Gene Ther. 17 (2009) 1959–1966, http://dx.doi.org/10.1038/mt.2009.146.
[48] J.M. Cloyd, N.R. Malhotra, L. Weng, W. Chen, R.L. Mauck, D.M. Elliott, Material properties in unconfined compression of human nucleus pulposus, injectable hyaluronic acid-based hydrogels and tissue engineering scaffolds, Eur. Spine J. 16 (2007) 1892–1898.
[49] J.C. Iatridis, L.A. Setton, M. Weidenbaum, V.C. Mow, The viscoelastic behavior of the non-degenerate human lumbar nucleus pulposus in shear, J. Biomech. 30 (1997) 1005–1013.
[50] M. Oyen, Mechanical characterisation of hydrogel materials, Int. Mater. Rev. 59 (2014) 44–59.
[51] J.M. Cloyd, N.R. Malhotra, L. Weng, W. Chen, R.L. Mauck, D.M. Elliott, Material properties in unconfined compression of human nucleus pulposus, injectable hyaluronic acid-based hydrogels and tissue engineering scaffolds, Eur. Spine J. Off. Publ. Eur. Spine Soc. Eur. Spinal Deform. Soc. Eur. Sect. Cerv. Spine Res. Soc. 16 (2007) 1892–1898, http://dx.doi.org/10.1007/s00586-007-0443-6.
[52] J.P. Gong, Y. Katsuyama, T. Kurokawa, Y. Osada, Double-network hydrogels with extremely high mechanical strength, Adv. Mater. 15 (2003), http://dx.doi.org/10.1002/adma.200304907, 1155-+.
[53] J.C. Iatridis, M. Weidenbaum, L.A. Setton, V.C. Mow, Is the nucleus pulposus a solid or a fluid? Mechanical behaviors of the nucleus pulposus of the human intervertebral disc, Spine 21 (1996) 1174–1184.
[54] H.J. Wilke, P. Neef, M. Caimi, T. Hoogland, L.E. Claes, New in vivo measurements of pressures in the intervertebral disc in daily life, Spine 24 (1999) 755–762.
[55] P.Y. Hwang, J. Chen, L. Jing, B.D. Hoffman, L.A. Setton, The role of extracellular matrix elasticity and composition in regulating the nucleus pulposus cell phenotype in the intervertebral disc: a narrative review, J. Biomech. Eng. 136 (2014) 021010.
[56] C.J. Hunter, J.R. Matyas, N.A. Duncan, The functional significance of cell clusters in the notochordal nucleus pulposus: survival and signaling in the canine intervertebral disc, Spine 29 (2004) 1099–1104.
[57] C.L. Gilchrist, E.M. Darling, J. Chen, L.A. Setton, Extracellular matrix ligand and stiffness modulate immature nucleus pulposus cell-cell interactions, PloS One 6 (2011) e27170.
[58] C.J. Hunter, J.R. Matyas, N.A. Duncan, The three-dimensional architecture of the notochordal nucleus pulposus: novel observations on cell structures in the canine intervertebral disc, J. Anat. 202 (2003) 279–291.
[59] H.A. Lin, M.S. Gupta, D.M. Varma, M.L. Gilchrist, S.B. Nicoll, Lower crosslinking density enhances functional nucleus pulposus-like matrix elaboration by human mesenchymal stem cells in carboxymethylcellulose hydrogels, J. Biomed. Mater. Res. Part A 104 (2016) 165–177.
[60] E.C. Collin, S. Grad, D.I. Zeugolis, C.S. Vinatier, J.R. Clouet, J.J. Guicheux, et al., An injectable vehicle for nucleus pulposus cell-based therapy, Biomaterials 32 (2011) 2862–2870.
[61] W.S. Toh, T.C. Lim, M. Kurisawa, M. Spector, Modulation of mesenchymal stem cell chondrogenesis in a tunable hyaluronic acid hydrogel microenvironment, Biomaterials 33 (2012) 3835–3845.
[62] J.-P. Draye, B. Delaey, A. Van de Voorde, A. Van Den Bulcke, B. De Reu, E. Schacht, In vitro and in vivo biocompatibility of dextran dialdehyde cross-linked gelatin hydrogel films, Biomaterials 19 (1998) 1677–1687.
[63] B. Reid, M. Gibson, A. Singh, J. Taube, C. Furlong, M. Murcia, et al., PEG hydrogel degradation and the role of the surrounding tissue environment, J. Tissue Eng. Regen. Med. 9 (2015) 315–318.
[64] G. Vadalà, G. Sowa, M. Hubert, L.G. Gilbertson, V. Denaro, J.D. Kang, Mesenchymal stem cells injection in degenerated intervertebral disc: cell leakage may induce osteophyte formation, J. Tissue Eng. Regen. Med. 6 (2012) 348–355, http://dx.doi.org/10.1002/term.433.
[65] J. Elisseeff, K. Anseth, D. Sims, W. McIntosh, M. Randolph, R. Langer, Transdermal photopolymerization for minimally invasive implantation, Proc. Natl. Acad. Sci. U. S. A. 96 (1999) 3104–3107.
[66] Y. Yang, J. Zhang, Z. Liu, Q. Lin, X. Liu, C. Bao, et al., Tissue-integratable and biocompatible photogelation by the imine crosslinking reaction, Adv. Mater. 28 (2016) 2724–2730, http://dx.doi.org/10.1002/adma.201505336.
[67] D.R. Griffin, W.M. Weaver, P.O. Scumpia, D. Di Carlo, T. Segura, Accelerated wound healing by injectable microporous gel scaffolds assembled from annealed building blocks, Nat. Mater. 14 (2015) 737–744.
[68] A.T. Francisco, R.J. Mancino, R.D. Bowles, J.M. Brunger, D.M. Tainter, Y.-T. Chen, et al., Injectable laminin-functionalized hydrogel for nucleus pulposus regeneration, Biomaterials 34 (2013) 7381–7388.
[69] L. Mosekilde, J. Kragstrup, A. Richards, Compressive strength, ash weight, and volume of vertebral trabecular bone in experimental fluorosis in pigs, Calcif. Tissue Int. 40 (1987) 318–322, http://dx.doi.org/10.1007/bf02556693.
[70] O. Lundin, L. Ekström, M. Hellström, S. Holm, L. Swärd, Exposure of the porcine spine to mechanical compression: differences in injury pattern between adolescents and adults, Eur. Spine J. 9 (2000) 466–471, http://dx.doi.org/10.1007/s005860000164.
[71] H. Tao, Y. Zhang, C-f Wang, C. Zhang, X-m Wang, D-l Wang, et al., Biological evaluation of human degenerated nucleus pulposus cells in functionalized self-assembling peptide nanofiber hydrogel scaffold, Tissue Eng. Pt A 20 (2014) 1621–1631.
[72] A. Schmocker, A. Khoushabi, C. Schizas, P.-E. Bourban, D.P. Pioletti, C. Moser, Miniature probe for the delivery and monitoring of a photopolymerizable material, J. Biomed. Opt. 20 (2015), 127001-.
[73] A. Schmocker, A. Khoushabi, D.A. Frauchiger, B. Gantenbein, C. Schizas, C. Moser, et al., A photopolymerized composite hydrogel and surgical implanting tool for a nucleus pulposus replacement, Biomaterials 88 (2016) 110–119, http://dx.doi.org/10.1016/j.biomaterials.2016.02.015.
[74] D.M. Elliott, C.S. Yerramalli, J.C. Beckstein, J.I. Boxberger, W. Johannessen, E.J. Vresilovic, The effect of relative needle diameter in puncture and sham injection animal models of degeneration, Spine 33 (2008) 588–596.
[75] J.-L. Wang, Y.-C. Tsai, Y.-H. Wang, The leakage pathway and effect of needle gauge on degree of disc injury post anular puncture: a comparative study using aged human and adolescent porcine discs, Spine 32 (2007) 1809–1815.